

Divertor flow asymmetries in helical devices: experimental results and relation to particle losses

V.V. Chechkin^a, M.S. Smirnova^a, L.I. Grigor'eva^a, E.L. Sorokovoy^a,
T. Mizuuchi^b, S. Masuzaki^c, K. Yamazaki^c

^aInstitute of Plasma Physics, National Science Center

“Kharkov Institute of Physics and Technology”, Kharkov, Ukraine.

^bInstitute of Advanced Energy, Kyoto University, Gokasho, Uji, Japan.

^cNational Institute for Fusion Science, Toki, Japan.

Abstract. The measured spatial distributions of plasma flows in the natural helical divertors of the $l = 2$ Heliotron E heliotron with ECH and NBI plasmas and $l = 3$ Uragan-3M torsatron with RF heated plasmas exhibit a strong vertical (up-down) asymmetry. The main characteristics of the asymmetry are: (1) a many-fold difference in the values of ambipolar flows in divertor legs symmetric about the torus midplane, (2) opposite polarity of non-ambipolar flows in these legs. In the Uragan-3M case, the larger ambipolar flow and the non-ambipolar flow with an excess of ions are always directed with the ion $\mathbf{B} \times \nabla B$ drift. In the Heliotron E case, a similar correspondence took place at a low heating power, and reversal of non-ambipolar flow polarity in the top and bottom parts of the torus was observed with heating power increase. As numerical simulations of particle direct losses in Uragan-3M have shown, the angular distributions of these losses agree qualitatively with the measured poloidal distributions of diverted plasma flows, the ion toroidal $\mathbf{B} \times \nabla B$ drift really being a main reason for the asymmetry of these losses. The account of the electric field E_r does not reverse the direction of the asymmetry. It follows from the heating power dependence of the divertor flow magnitude that some initial, not heating-associated flow asymmetry existed in Heliotron E. This initial asymmetry was supposedly caused by magnetic field distortions in the divertor layer. A further $\mathbf{B} \times \nabla B$ drift-caused increase of the asymmetry with heating could be enhanced considerably due to the natural vertical asymmetry of helical magnetic field ripple, which is inherent to all $l = 2$ helical systems. A substantial modification of the divertor flow up-down asymmetry observed in Heliotron E with heating power increase, including reversal of the ambipolar flow polarity, could occur under the effect of E_r field and its shear on escaped particle orbits.

Contents

1. Introduction.
2. Main manifestations of vertical asymmetry of plasma flows in the divertor regions of the Heliotron E and Uragan-3M helical devices.
 - 2.1. Experimental conditions on H-E and U-3M.
 - 2.2. Poloidal distributions of divertor flows in the symmetric poloidal cross-sections of H-E and U-3M.
 - 2.2.1. Ambipolar flows.
 - 2.2.2. Non-ambipolar flows.
 - 2.3. Plasma heating effects on divertor flow asymmetry in H-E.
 - 2.3.1. Neutral beam injection.
 - 2.3.2. Electron cyclotron heating.
 - 2.3.3. The effect of plasma heating on non-ambipolar divertor flows.
3. Relation of divertor flow asymmetry to direct particle losses.
 - 3.1. Relation of divertor flow asymmetry to direct losses of charged particles in U-3M.

- 3.2. Effects of magnetic field parameters on particle losses and divertor flow asymmetry in H-E and other stellarator-type devices.
 - 3.2.1. Effects of toroidicity and satellite harmonic content of the helical magnetic field.
 - 3.2.2. Effects of magnetic axis shift.
 - 3.2.3. Effects of distant magnetic field harmonics created by additional toroidal field.
- 3.3. Possible impact of E_r on divertor flow asymmetry in H-E.
- 3.4. Predictions of fast particle behavior in the SOL region: effects of magnetic field parameters and heating conditions.

4. Summary.

1. Introduction

In diverted tokamak experiments a many-fold difference is always observed in the values of power flux flowing to the target plates and, consequently, in divertor plasma characteristics in the inner and outer legs of the divertor (“horizontal, or in-out, asymmetry”, see, e.g., Ref. [1]) or in the legs positioned over and under the torus midplane (“vertical, or up-down, asymmetry”) [2, 3]. Reversal of toroidal magnetic field direction alters characteristics of these asymmetries [3], this being an indication of plasma drift effects. It has been shown [3,4] that the $\mathbf{E} \times \mathbf{B}$, $\mathbf{B} \times \nabla B$, $\mathbf{B} \times \nabla P$ and $\mathbf{B} \times \nabla T$ drifts in the edge plasma of a tokamak can really be responsible for the asymmetry of particle and heat fluxes entering the divertor and, consequently, for the imbalance in subsequent physical processes developing in the divertor (recycling, occurrence of cold radiative plasma, detachment). Also, it has been shown [2,5] that a certain contribution to the divertor asymmetry in a tokamak can be made by suprathermal (“epithermal” and runaway) electrons exhausted from the confinement volume. Apart from asymmetry-causing mechanisms connected with particle dynamics, distortions of the real divertor magnetic configuration by small error fields could be an initial reason for the asymmetry (for example, a separation of the separatrix surface into “inner” and “outer” separatrices in a double-null tokamak divertor [6]).

Diverted field lines are natural components of any heliotron/torsatron edge magnetic configuration. In such a configuration bundles of diverted field lines deviate from the separatrix region into the space between the helical coils and this can be used for realization of helical divertor. A detailed numerical modeling of the natural divertor magnetic configuration and an analysis of possible operating regimes of the helical divertor for the $l=2$ Large Helical Device (LHD) heliotron were presented in Ref. [7], and the first results of experimental studies of this LHD divertor have been published in Ref. [8].

Besides, detailed experimental studies of spatial distributions of diverted plasma flows carried out on the $l=2$ Heliotron E (H-E) heliotron have shown [9–11] that a strong vertical asymmetry of divertor flows can be inherent to helical devices just as to tokamaks. This conclusion has been confirmed by measurements of divertor flow distributions in the $l=3$ Uragan-3M (U-3M) torsatron [12].

The presence of many-fold difference in the values of particle and heat flows entering different regions of the divertor facility in both tokamaks and stellarator-type devices is of prime importance for the design of this facility and the choice of its operating regime in large devices of ITER scale, where the maximum energy load on the target plates cannot exceed several MW/m² for technological reasons. Therefore, the search for physical mechanisms, which are responsible for the asymmetry of divertor flows, and for methods of asymmetry correction should become a highly important object of divertor research.

This paper overviews some results of experimental studies of vertical asymmetry of spatial distributions of plasma flows in the divertor regions of H-E and U-3M. Besides, results have been cited of theoretical and numerical analysis of angular distributions of direct charged particle losses in devices of such type. It follows from comparison of experimental and theoretical results that the distributions of divertor flows and particle losses, the asymmetries of both these distributions, qualitatively agree. In general, both kinds of asymmetry, vertical and horizontal, can exist

simultaneously in the natural helical divertor of a torsatron/heliotron. However, only the vertical asymmetry has been examined more or less in detail in H-E and U-3M. A juxtaposing of research results from two stellarator-type devices differing substantially by their magnetic configuration and methods of plasma heating allows one to reveal in more detail main characteristics of the divertor flow asymmetry in helical devices, its physical reasons and ways of asymmetry reduction.

In both devices, the spatial distributions of diverted plasma flows were measured with plane electric probe arrays, which were arranged poloidally in the spacings between the helical coils in several poloidal cross-sections of the torus. The measurements were carried out at relatively low values of plasma density \bar{n}_e ($1\text{--}3 \times 10^{19} \text{ m}^{-3}$ in H-E, units of 10^{18} m^{-3} in U-3M). Therefore, such effects as recycling, cold plasma formation with conversion of a substantial fraction of the exhausted power into radiation, plasma detachment were negligible in the divertor region [13]. In this sense, divertor plasma parameters measured by the probes were directly related to plasma parameters in the upstream flow and to processes developing in the confinement volume. As a measure of diverted plasma flow magnitude, either the ion saturation current I_s to a probe (the current to a negatively $\sim 100\text{--}200 \text{ V}$ biased probe) [10–12] or the current I_p to a grounded probe (the current to a probe electrically short-circuited to the chamber wall, “plasma current”) [12, 14] were taken. In the former case, the divertor flow magnitude is estimated as if the flow hit an electrically isolated target plate (“ambipolar divertor flow”). The latter case corresponds to conditions where a target plate is electrically short-circuited to the wall. Since a potential difference exists between the plasma and the wall (grounded probe), the detected plasma flow is essentially non-ambipolar with an excess of either ions or electrons in it (the sign of dominating particle charge definitely agrees with the floating potential V_f polarity). The spatial distribution of plasma current is closely linked with physical processes in the SOL and confined plasmas. Therefore, studies of this current also facilitate understanding of the asymmetry nature.

In the most simple and clear presentation, the main characteristics of the vertical asymmetry of divertor flows in a helical device can be exposed in so-called symmetric poloidal cross-sections of the torus where the helical coils and the footprints of calculated field line trajectories (Poincare plots) of the “ideal” divertor magnetic configuration in the upper and lower halves of the torus are disposed symmetrically about the midplane. In H-E ($l=2$, $m=19$) there were two such cross-sections in each field period separated toroidally by the half field period, $(0^\circ/m)$ and $(180^\circ/m)$, or $(0^\circ/9.5)$ and $(90^\circ/9.5)$, respectively (Fig. 1, the Ref. [15] notations are used). Similar cross-sections in U-3M ($l=3$, $m=9$) are half field period-separated cross-sections $\phi = 0^\circ$ (A-A) and $\phi = 20^\circ$ (D-D) (Fig. 2). The divertor magnetic configurations in the $(0^\circ/m)$ cross-section in H-E and in the A-A cross-section, top and bottom, in U-3M are similar to that of a symmetric double-null divertor in a tokamak (e.g., in the TdV tokamak [6]), while the configurations on the outboard side of the torus in the $(180^\circ/m)$ and D-D cross-sections are similar to that of symmetric single-null divertors in the JFT-2a (DIVA) [2] and TEXT-Upgrade [3] tokamaks. Away from the symmetric cross-sections, divertor field line distributions, which have the same form in the upper and lower halves of the torus, lie in different poloidal cross-sections. Therefore, corresponding distributions of diverted plasma flows can also be subjected, in principle, to some toroidal asymmetry [16].

2. Main manifestations of vertical asymmetry of plasma flows in the divertor region of the Heliotron E and Uragan-3M helical devices

2.1. Experimental conditions on H-E and U-3M

In the Heliotron E device ($l=2$, $m=19$, $R_0=2.2 \text{ m}$, $\bar{a} \approx 0.2 \text{ m}$, $B_\phi = 1.9 \text{ T}$, $\iota(\bar{a})/2\pi \approx 2.5$) the inner radius of the rounded parts of the vacuum chamber was 0.41 m , so the whole region of X-points was inside the chamber and two well-separated diverted magnetic fluxes fell at the wall in all considered spacings between the helical coils (Fig. 1). The basic studies of corresponding plasma flows were carried out with the toroidal magnetic field produced by the helical coils only and

directed clockwise (“negative magnetic field”, the ion $\mathbf{B} \times \nabla B$ drift caused by toroidicity (further on, “toroidal drift”) is directed downward. A “currentless” plasma was produced by fundamental ECH (ECH-1: 53.2 GHz, irradiated power up to 0.4 MW) and second harmonic ECH (ECH-2: 106.4 GHz, 0.3 MW). After this, it was supported and heated by neutral beam injection (NBI) from several beam lines with the 23–24 kV injection voltage, the injection angles 62°, 79° and 90° and the total injected power up to 3 MW. In some cases, an additional ECH pulse was imposed on NBI. Typical values of density \bar{n}_e were $(1-3) \times 10^{19} \text{ m}^{-3}$, the plasma temperature ranged within 0.6–1.5 keV for $T_e(0)$ and 0.3–0.6 keV for $T_i(0)$.

To study the diverted plasma in H-E, 56 collecting plates (CP) were used [9], each plate being $5 \times 0.8 \text{ cm}^2$ in size. The plates were divided into eight 7-plate arrays with the plate numbers 1, 2, ..., 7 in each array. The arrays were arranged poloidally on both rounded parts of the vacuum chamber in four poloidal cross-sections with the interval of 1/4 field pitch, including the symmetric cross-sections ($0^\circ/m$) and ($180^\circ/m$) (Fig. 1).

In the Uragan-3M torsatron ($l = 3$, $m = 9$, $R_0 = 1 \text{ m}$, $\bar{a} \approx 0.1 \text{ m}$, $B_\phi = 0.7 \text{ T}$, $\iota(\bar{a})/2\pi \approx 0.4$), the whole magnetic system is enclosed into a large 5 m diameter vacuum chamber, so an open helical divertor is realized in this device. A “currentless” plasma with the density of $\bar{n}_e \approx 2 \times 10^{18} \text{ m}^{-3}$ is produced and heated by RF fields ($\omega \approx \omega_{ci}$), the irradiated power being $\sim 200 \text{ kW}$. The temperature of the main group of electrons is $T_e \approx 0.3 \text{ eV}$ with a minor group of suprathermal ($\geq 1 \text{ keV}$) electrons at the confined plasma periphery [17]. The temperature of the main group of ions is $T_i \approx 0.1 \text{ keV}$. Also, two minor groups of hotter ions are recorded with the temperatures of 0.2–0.3 and 0.6–0.8 keV, respectively.

The flows of diverted plasma in U-3M are detected by 78 plane Langmuir probes, each being $1.25 \times 0.77 \text{ cm}^2$ in size. The probes are grouped in 6 arrays, which are arranged poloidally in the spacings between the helical coils at a minor radius of $r = 27 \text{ cm}$ exceeding the X-point radius $r_x \sim 20 \text{ cm}$ in two adjacent symmetric poloidal cross-sections A-A and D-D (Fig. 2). The measurements of diverted plasma parameters were carried out in the toroidal magnetic field directed both clockwise (“negative magnetic field”, with the toroidal ion $\mathbf{B} \times \nabla B$ drift directed downward) and counterclockwise (“positive magnetic field”).

2.2. Poloidal distributions of divertor flows in the symmetric poloidal cross-sections of H-E and U-3M

2.2.1. Ambipolar flows

Poloidal distributions of ambipolar flows of diverted plasma in the top and bottom spacings of the ($0^\circ/m$) cross-section and in the outboard spacing of the ($180^\circ/m$) cross-section in H-E are presented in Fig. 3 as $I_s(N)$ plots [11]. Similar dependencies measured in the top and bottom spacings of the cross-section A-A and in the outboard spacing of the cross-section D-D in U-3M are shown in Fig. 4 [12]. The data for H-E in Fig. 3 were taken at relatively simple conditions where the plasma was heated by NBI from a single injection line with a comparatively low power of the injected beam, $P_{inj} \approx 0.7 \text{ MW}$, and the inlet position being nearly toroidally symmetric about the CP arrays. Also, in Fig. 3 presented are calculated poloidal distributions of the connection length L of open field lines with the starting points lying along the lines of CP array disposition [10, 11]. In the U-3M case, the data in Fig. 4 are presented for both negative (left column) and positive (right column) directions of the magnetic field.

Basing on the calculations of diverted field line trajectories (Fig. 1) and connection lengths (Fig. 3) for H-E, one should expect the most intense plasma flows to be picked up by the plates $N = 2, 3, 5$ at the top and bottom in the cross-section ($0^\circ/m$) and by the plates $N = 2$ and $N = 6$ over and under the midplane, respectively, on the outboard side in the cross-section ($180^\circ/m$). The really measured $I_s(N)$ distributions at the top and bottom in the cross-section ($0^\circ/m$) appreciably differ in their form. However, the main characteristic of the vertical asymmetry of the divertor flows in this

cross-section is a many-fold difference in the flow magnitude in the symmetrically positioned divertor legs. In particular, the current I_s to the plate $N = 5$ at the bottom is ~ 50 times higher than that to the plate $N = 5$ at the top. For these data, the asymmetry index defined as $\Delta_s = (I_s^{bott} - I_s^{top}) / (I_s^{bott} + I_s^{top})$ is 0.96, that is, it is close to its ultimate value 1. With this, the larger divertor flow is directed with the ion toroidal drift. At the same time, the plasma flows symmetrically positioned near the midplane in the cross-section ($180^\circ/m$) are comparable in their magnitude, and the flow picked up by the plate $N = 2$ over the midplane is even 1.4 times higher than the flow picked up by the plate $N = 6$ under the midplane ($\Delta_s = -0.24$, a possible interpretation is given below, Sec. 2.3.1). With account of the character of I_s distributions, measured on the outboard side in the intermediate cross-sections ($90^\circ/m$) and ($270^\circ/m$) [11] (not shown here), we may conclude that the degree of the vertical asymmetry of divertor flows in H-E is the highest at the maximum distance from the midplane and decreases with approaching it.

As follows from the form of $I_s(N)$ distributions for U-3M (Fig. 4), of two plasma flows at the top and bottom of the cross-section A-A, the larger one is located closer to the major axis of the torus (“inner flow”). This is in a qualitative agreement with the calculated distributions of the density of footprints of diverted field lines in U-3M [12,18] (the same regularity holds also for the D-D cross-section). Note that a similar characteristic is also observed in H-E (see Fig. 1). The $I_s(N)$ distributions in the A-A cross-section of U-3M also exhibit a vertical asymmetry, though not as strong as in H-E. In the negative magnetic field case, the inner flow at the bottom is not less than 2.6 times higher than the inner flow at the top ($\Delta_s \geq 0.45$). With reversal of the magnetic field direction, the larger flow goes to the top. Thus, in the U-3M case, with any magnetic field direction, the larger divertor flow is directed with the ion toroidal drift. On the outboard side of the D-D cross-section in U-3M, in the negative magnetic field case, the larger plasma flow appears under the midplane, i.e., on the ion toroidal drift side, being in ~ 2 fold excess of the upper flow. The splitting of the larger I_s maximum is an additional element of asymmetry, whose nature needs a special study. In the positive magnetic field case, the larger I_s maximum goes to the upper half of the torus, retaining its splitting.

2.2.2. Non-ambipolar flows

Besides the dominating outflow of the diverted plasma being in the direction of the ion toroidal drift under Fig. 3 and Fig. 4 conditions, the character of poloidal distributions of non-ambipolar divertor flows in H-E [14] and U-3M [12] also evidences that the ion motion makes an appreciable contribution to the vertical asymmetry of the divertor flows. These distributions are presented as $I_p(N)$ plots in Figs. 5, 6 for the same conditions as those for the Figs. 3, 4 plots. In the cross-section ($0^\circ/m$) of H-E (Fig. 5), the non-ambipolar flow with an excess of ions ($I_p > 0$) to the plate $N = 5$ at the bottom corresponds to the larger ambipolar flow of two ones hitting the symmetrically positioned plates $N = 5$ at the top and bottom (cf. Fig. 3). At the same time, the electrons dominate ($I_p < 0$) in the non-ambipolar flow collected by the plate $N = 5$ at the top. In the cross-section ($180^\circ/m$), a positive plasma current also corresponds to the ambipolar flow going under the midplane ($N = 6$), while the plasma current collected by the symmetrically positioned plate $N = 2$ over the midplane is negative. The similar correspondence takes place in the U-3M case (Fig. 6). Here, with reversal of the magnetic field direction accompanied by reversal of the asymmetry of ambipolar flows in their magnitude (Fig. 4), the corresponding non-ambipolar flows undergo reversal in their sign.

2.3. Plasma heating effects on divertor flow asymmetry in H-E

In both U-3M with RF heated plasmas [19,20] and H-E under NBI, ECH and combined NBI+ECH heating conditions [10,11], the ambipolar flows of diverted plasma grow with heating power. Such dependence is considered as a manifestation of a common for tokamaks and

stellarators regularity, power degradation of confinement [21]. The dependencies of divertor flow magnitude on the heating power and the method of heating having been studied on H-E enable one to find out effects of heating on the vertical asymmetry of the divertor flows and to understand, to some extent, possible reasons for the asymmetry in helical systems.

2.3.1. Neutral beam injection

The plots of density-normalized ion saturation current I_s/\bar{n}_e versus density-normalized total (i.e., summed over all methods of heating) absorbed power P_{abs}/\bar{n}_e are shown in Fig. 7 (cross-section ($0^\circ/m$), the inner legs at the top and bottom) and Fig. 8 ($(180^\circ/m)$, outboard spacing) [11]. Similar dependencies for the current I_s summed over all the CPs in the upper or lower parts of each cross-section are shown in Fig. 6 of Ref. [10]. In Figs. 7 and 8, the data for all heating regimes used in divertor studies are collected (ECH, NBI, NBI+ECH). The interpolating straight lines are drawn through the NBI-only points (●). When extrapolated toward parameter P_{abs}/\bar{n}_e decrease, the straight lines cross the vertical axis at some initial values of $I_s/\bar{n}_e = (I_s/\bar{n}_e)_0$, which, in general, differ from zero and, also, differ by their value in symmetrically positioned divertor legs in the upper and lower halves of the torus. This means that some initial, not heating-associated vertical asymmetry could exist. The index of this asymmetry was already close to unity. It follows from Fig. 7 that with NBI power rise, the difference between I_s/\bar{n}_e values in the top and bottom legs in the cross-section ($0^\circ/m$) also rose. In this sense, the asymmetry increased with heating. With the maximum value of normalized power $P_{\text{abs}}/\bar{n}_e \approx 600 \text{ kW}/10^{19} \text{ m}^{-3}$ attained in these studies, the heating-induced I_s/\bar{n}_e increment in the bottom leg was comparable with $(I_s/\bar{n}_e)_0$. Near the midplane in the $(180^\circ/m)$ cross-section (Fig. 8), the initial asymmetry of the flows was directed opposite to that in the $(0^\circ/m)$ cross-section (cf. Fig. 7). However, with heating power increase, the difference between the flow magnitudes at the top and bottom was reduced. Proceeding from the Fig. 8 plots, we may expect that this difference became zero at $P_{\text{abs}}/\bar{n}_e \approx 600 \text{ kW}/10^{19} \text{ m}^{-3}$, and with further P_{abs}/\bar{n}_e increase, the asymmetry was expected to develop in the same direction as at the largest distance from the midplane, in the cross-section ($0^\circ/m$).

By analogy with double-null divertor in a tokamak [6], distortions of the real divertor magnetic configuration could be a reason for the initial vertical asymmetry of divertor flows in H-E. Such distortions might occur, for example, due to a minor deformation or shift of the helical coils in the process of their long exploitation and result in an additional ergodization of field lines and a separation of magnetic surfaces at the periphery. On the other hand, the further amplification and modification of the asymmetry with plasma heating should be related to specifics of particle dynamics in the confinement volume, the character of particle losses and the effects of radial electric field on these losses (see below, Sec. 3). Thus, in general case, the observed vertical asymmetry of divertor flow distributions in H-E can be considered as being formed by two components. In the $(0^\circ/m)$ cross-section both components have the same direction, while on the outboard side of the $(180^\circ/m)$ cross-section they are directed oppositely. If the proposed hypothesis concerning the origin of initial asymmetry is really valid, then with reversal of the magnetic field direction, this asymmetry would not reverse, while the heating-induced toroidal drift-associated asymmetry component would alter its direction, by analogy with the U-3M case, and in part or completely balance the initial asymmetry. Probably, this is why a relaxation of the vertical asymmetry was observed in H-E with magnetic field reversal [10].

Probably, it is the presence of non-zero value of $(I_s/\bar{n}_e)_0$ for the flow over the midplane in the cross-section $(180^\circ/m)$ (Fig. 8) that can explain the excess of current $I_s(2)$ (i.e., over the midplane) above the current $I_s(6)$ (i.e., under the midplane) in Fig. 3, contrary to what has been observed in the D-D cross-section of U-3M in the negative magnetic field case (Fig. 4).

2.3.2. Electron cyclotron heating

It follows from Fig. 7 that for the bottom inner leg in the ($0^\circ/m$) cross-section the $I_s/\bar{n}_e - P_{\text{abs}}/\bar{n}_e$ points obtained with the use of ECH, namely, ECH-1 (\circ), ECH-2 (\square), NBI+ECH-1 (\oplus), NBI+ECH-2 (\boxplus), NBI+ECH-1+ECH-2 (\boxtimes), within the data spread follow in average the straight line drawn through the NBI-only points. At the same time, for the symmetrically positioned leg at the top the points with ECH-1 systematically deviate upward from this line. In the outboard spacing of the ($180^\circ/m$) cross-section (Fig. 8), all the ECH points for the leg over the midplane ($N = 2$) follow the straight line in average, while for the leg under the midplane ($N = 6$) the ECH-1 points also exhibit a systematical deviation upward. Thus, in both symmetric poloidal cross-sections the fundamental ECH resulted in an enhanced plasma outflow to the lesser of the two symmetrically positioned flows. At the same time, the second harmonic ECH (ECH-2, NBI+ECH-2) was not accompanied by an enhanced outflow of the plasma to the divertor region as compared with the NBI-only case. Such a difference in the effect of two kinds of ECH on the divertor flows, their asymmetry, could be associated with the difference in power deposition profiles caused, in turn, by the difference in launching systems for ECH-1 and ECH-2 [22]. In the ECH-1 case, a substantial fraction of the injected microwave power was deposited at the confined plasma periphery, while in the ECH-2 case, the main power was absorbed in the central region, thus creating a peaked T_e profile.

An enhanced, as compared with NBI, particle escape into the divertor region with peripheral plasma heating by fundamental ECH, at least partially, had a convection-like (i.e., non-diffusive) character. This was evidenced by the form of current I_s time variation when a short (25 ms) ECH-1 pulse was imposed on a long NBI (see insets in Figs. 7,8). A distinct deviation of ECH-1 points from the straight line (the top flow in the ($0^\circ/m$) cross-section, the flow under the midplane in the ($180^\circ/m$) cross-section) correlated with the presence of fast (~ 1 ms or less) phase of I_s increase after the additional ECH-1 switched on. In those flows where the ECH-1 points followed the straight line (the bottom flow in the ($0^\circ/m$) cross-section, the flow over the midplane in the ($180^\circ/m$) cross-section), only a slow I_s rise, its time being comparable with the ECH-1 pulse length or with the confinement time, was observed with additional ECH-1 switched on, evidencing a diffusive character of particle outflow in these cases. With a short ECH-2 pulse imposed on NBI, only a slow, diffusion-like I_s rise was observed in all the divertor flows considered.

2.3.3. The effects of plasma heating on non-ambipolar divertor flows

The $I_p/\bar{n}_e - P_{\text{abs}}/\bar{n}_e$ plots are shown in Fig. 9(a) (inner ($0^\circ/m$) legs) and Fig. 10 (outboard ($180^\circ/m$) legs) [14]. Here, just as in the case of similar plots for I_s (Figs. 7,8), the extrapolating straight lines are drawn through the NBI-only points (\circ at the top and \bullet at the bottom). Despite a considerable data spread, it is seen in Fig. 9(a) that with normalized power increase, reversal of plasma current direction in both inner ($0^\circ/m$) legs occurred at $P_{\text{abs}}/\bar{n}_e \approx 200\text{--}300 \text{ kW}/10^{19} \text{ m}^{-3}$. With a further P_{abs}/\bar{n}_e increase, the electrons dominated in the non-ambipolar flow, which corresponded to the larger ambipolar flow (i.e., at the bottom). A several times-repeated plasma current reversal in the bottom leg with different regimes of plasma heating is evidently demonstrated in one operating shot in Fig. 9(b). Here, in the process of plasma production by ECH and its subsequent heating by NBI, NBI+ECH and NBI+NBI the current I_p changed its direction five times, depending on the value of the P_{abs}/\bar{n}_e parameter. On the outboard side in the ($180^\circ/m$) cross-section (Fig. 10), a monotonous rise of $|I_p/\bar{n}_e|$ (supposedly, from zero) within the available range of P_{abs}/\bar{n}_e values took place in both divertor legs without changing the sign of I_p .

It follows from the plots presented in Fig. 9 that at a sufficiently high heating power ($P_{\text{abs}}/\bar{n}_e > 200\text{--}300 \text{ kW}/10^{19} \text{ m}^{-3}$) the toroidal drift itself became no more a dominating factor in

formation of the vertical asymmetry of divertor flow distributions in H-E. In these conditions, to understand the nature of the heating-associated vertical asymmetry component, other factors, namely, those which could result in the dominating shift of electrons to the lower part and ions to the upper part of the plasma column, should be put into consideration. The analysis of the form of current I_p and/or potential V_f time variation in divertor legs with transition from $P_{\text{abs}}/\bar{n}_e < 200\text{--}300 \text{ kW}/10^{19} \text{ m}^{-3}$ to $P_{\text{abs}}/\bar{n}_e > 200\text{--}300 \text{ kW}/10^{19} \text{ m}^{-3}$ could facilitate such an understanding. Figure 11 demonstrates how the potential of isolated collecting plates changed during such a transition, when either a shorter NBI (Fig. 11, left column) or a shorter ECH-1 (Fig. 11, right column) pulse was imposed on a long NBI [14]. The signals of the current I_p to the grounded plates had a qualitatively similar form. It is seen in Fig. 11 that in full accord with Fig. 9, with any kind of additional heating, the direction of outflow of dominant particles into the inner ($0^\circ/m$) legs changed from downward to upward for ions and from upward to downward for electrons, not depending on the method of additional heating. Generally, the transition contained two phases, fast and slow. More or less distinctly, the fast phase displayed itself in all cases shown in Fig. 11 with the exception of additional ECH-1 case in the top ($0^\circ/m$) leg. In the case of additional NBI, it is natural to relate the fast phase of V_f rise and the reversal of V_f polarity in the top ($0^\circ/m$) leg to a fast, convection-like occurrence of additional number of high-energy ions predominantly in the upper half of the torus and, possibly, their partial outflow into this leg. With this, the reversal of polarity and the drop of V_f in the bottom leg attributed to a dominating outflow of electrons followed more slowly. In the same way, in the additional ECH-1 case, the fast phase of V_f drop occurring in the ($0^\circ/m$) bottom leg could be attributed to a group of fast electrons born by ECH-1, moreover, at the plasma periphery. With this, there was no fast phase at all in the rise of V_f and reversal of V_f polarity in the ($0^\circ/m$) top leg, as if the additional outflow of ions into this leg was purely diffusive in its nature. In the case of additional ECH-1, it is noteworthy that on the outboard side in the ($180^\circ/m$) cross-section, the V_f variation possesses a distinctly pronounced fast phase, where the potential drops, contrary to its rise at the slow phase. This is one more corroboration that the fast and slow phases are related to different mechanisms of particle loss.

3. Relation of divertor flow asymmetry to direct particle losses

The character of I_s and I_p poloidal distributions in the divertor region of the U-3M torsatron with a fixed regime of RF heating, the vertical asymmetry of these distributions, with a larger I_s maximum being on the ion toroidal drift side and with an ion excess in the corresponding plasma current, is an evidence of a substantial effect on these distributions of convective (non-diffusive, or direct) losses of fast charged particles. It is known [23] that fast, suprathermal ions and electrons are mostly subjected to the toroidal drift in tokamaks, which is directed vertically and results in prompt escape of these particles from the confinement volume. Such fast particles can affect considerably the structure of divertor plasma flows in a tokamak [24]. As to a helical device, the more it deviates from the quasi-helical symmetry, the larger the fraction of vertically drifting and therefore poor confined charged particles (particles with toroidal banana orbits and barely helically ripple-trapped ones) is in this device. Therefore, effects of vertically drifting lost particles on divertor flow distributions should be also expected in helical configurations, which are far from quasi-helical symmetry. In particular, such a connection between the direct fast particle losses and the divertor flow asymmetry looks attractive for the non-drift-optimized U-3M configuration, where the presence of fast particles in plasma has been verified experimentally [12,17]. As will be shown below, the more optimized the helical configuration is from the view point of particle confinement, the lower asymmetry of direct particle loss distribution is inherent for such a configuration, and the lower effect of this asymmetry on divertor flow distribution should be expected.

A similar connection should be also expected for H-E, though the whole picture looks much more complicated in this case. Here, the initial (i.e., in the limit of zero heating power) vertical asymmetry of divertor flow distributions is assumed to result from distortions of the “ideal”

magnetic structure of the divertor layer [6,11]. With a low heating power, the ion toroidal drift and associated asymmetric direct particle losses similar to those in U-3M could be a new additional factor affecting the vertical asymmetry of divertor flows. However, in the H-E case, this factor was considerably enhanced by the natural vertical asymmetry of helical field ripple [25,26]. A possible impact of convective particle losses on the magnitude and distribution of divertor flows in H-E was evidenced by fast variations in the I_s and $V_f(I_p)$ responses to a fast rise of the heating power. With heating power increase, a growing effect of the ambipolar electric field E_r on the particle loss structure [27] and, consequently, on diverted plasma distribution should be expected.

The results obtained on U-3M are distinguished with larger simplicity in their interpretation than in the H-E case. Moreover, the measurements in U-3M were carried out for two directions of the toroidal magnetic field. This enables us to make a more grounded conclusion about the ion $\mathbf{B} \times \nabla B$ drift to be a main reason for the observed asymmetry. In view of this, we shall consider the link between divertor flow asymmetry and particle loss in helical systems, starting with the U-3M case.

3.1. Relation of divertor flow asymmetry to direct losses of charged particles in U-3M

In order to find out the character of direct losses of both thermal and fast charged particles in U-3M and a correspondence of the distribution of these losses to the measured distributions of divertor flows, a numerical simulation of trajectories of 3000-5000 test ions and electrons has been carried out with the use of the Monte-Carlo method [12]. The particle orbits were followed from the moment of their start on the $r/\bar{a} = 0.7$ magnetic surface to the last closed magnetic surface ($r/\bar{a} = 1$) intersection. The direct losses were analyzed for the total energy intervals of 0.1–0.5 keV for ions and 0.3-1.2 keV for electrons for both negative and positive magnetic field cases. In both cases, estimations were made of the effect of the radial electric field E_r , its value and profile were derived from the velocity of plasma poloidal rotation, the velocity, in turn, being inferred from the microwave reflectometric probing of the plasma [28].

It follows from the calculations that ions and electrons with transient orbits dominate among the lost particles. Being toroidally trapped on the starting surface, these particles, when drifting toward the boundary surface, tend to be trapped in the helical ripple wells near the vertical axis (Fig. 12(a,b)). Due to difference in the values of Larmor radius, the fraction of escaping ions is larger by an order of magnitude than that of electrons with the same energy. In the negative magnetic field case, the 0.7–1.2 keV electrons leave the confinement volume mainly in the upper half of the inner region of the torus in the spacings between the helical coils (Fig. 13(a)). The intersection of the boundary surface by typical orbits of escaping electrons is characterized by a highly peaked horizontally-asymmetric histogram in poloidal angle (Fig. 14(a)). Most of escaping ions have their poloidal co-ordinates of boundary intersection in the lower half of the torus (Figs. 13(b), 14(b)). The distribution over θ of intersection points possesses a distinct vertical asymmetry. This asymmetry is caused mainly by the magnetic field gradient and associated particle drift. In the positive magnetic field case, the dominating direction of particle escape from the confinement volume is reversed in comparison with the negative magnetic field case (Figs. 13, 14). Since the direct ion losses are larger than the electron losses, the vertical asymmetry of the flows of escaping ions is expected to make a determinative effect on the vertical asymmetry of divertor flows in U-3M.

The field E_r in U-3M (up to ~ 40 V/cm in absolute value [28]) practically does not affect the confinement of electrons, however, it substantially affects the ion confinement. In the negative magnetic field case, at the periphery where $E_r < 0$ [28] the condition of so-called helical resonance [29–31] is fulfilled, $\Omega_{\nabla B} + \Omega_{E \times B} \approx 0$, where $\Omega_{\nabla B} = cW\varepsilon_h/eBr^2$ is the frequency of the ion $\mathbf{B} \times \nabla B$ drift-associated poloidal precession, W is the particle energy, ε_h is the helical inhomogeneity of magnetic field, and $\Omega_{E \times B} = cE_r/(Br)$ is the poloidal rotation frequency due to the electric drift. Closeness of $\Omega_{\nabla B}$ and $\Omega_{E \times B}$ results in the mechanism of $\mathbf{B} \times \nabla B$ drift compensation by the $\mathbf{E}_r \times \mathbf{B}$ rotation no more

to work. In turn, this results in 20% rise of thermal ion (0.1 keV) loss and in 1.5-fold increase in the degree of asymmetry of the escaping ion flow in comparison with the $E_r = 0$ case. In the positive magnetic field case, $E_r > 0$ at the periphery [28]. Such an electric field facilitates delocalization from helical ripple wells of those ions, for which the condition of so-called toroidal resonance [30,31] is satisfied, $\Omega_T + \Omega_{E \times B} \approx 0$, where $\Omega_T = (v/2\pi)V_{\parallel}/R_0$. This results in smaller radial deviations of fast particles and, respectively, to a decrease of both lost ion fraction and the degree of asymmetry of lost ions flows. Nevertheless, the account of E_r does not lead to qualitative changes in the character of the asymmetry of lost ion flows in U-3M.

Thus, the calculated angular distributions of co-ordinates of ion outflow on the boundary surface in U-3M qualitatively agree with the measured distributions of the flows of diverted plasma in both negative and positive magnetic field cases.

3.2. Effects of magnetic field parameters on particle losses and divertor flow asymmetry in H-E and other stellarator-type devices

3.2.1. Effects of toroidicity and satellite harmonic content of the helical magnetic field

Apart from heating-independent plasma losses associated with distortions of the magnetic configuration, and neglecting E_r effects, the main particle losses in H-E, similar to those in U-3M, should be caused by fast toroidal banana-ions, which are trapped in the helical ripple wells at the plasma periphery [26,29,32], and the non-compensated ion $\mathbf{B} \times \nabla B$ drift should be a determinative mechanism of direct particle losses and the vertical asymmetry of poloidal distributions of these losses. However, in the H-E case, the degree of vertical asymmetry of fast ion loss distribution undergoes a many-fold increase due to the natural vertical asymmetry of the helical magnetic field ripple [25,26]. This kind of asymmetry differs from that caused by a single-null divertor in a tokamak or a vertical displacement of the plasma column [33] and is inherent, to a larger or lesser extent, to all $l = 2$ heliotrons/torsatrons. It results from the difference in the value of satellite helical harmonics $\varepsilon_{l-1,1}$ and $\varepsilon_{l+1,1}$ nearest to the main harmonic $\varepsilon_{l,1}$ in the Fourier series of the magnetic field and is an exhibition of deviation of these configurations from quasi-helical symmetry.

The character of poloidal modulation of the helical ripple in an asymmetric configuration is adequately described by two parameters, $\sigma = (\varepsilon_{l-1,1} + \varepsilon_{l+1,1})/\varepsilon_{l,1}$ and $\bar{\sigma} = (\varepsilon_{l-1,1} - \varepsilon_{l+1,1})/\varepsilon_{l,1}$ [24] characterizing the degree of horizontal and vertical asymmetry, respectively. In the case of vertically symmetric configuration, $\bar{\sigma} = 0$. A strong vertical asymmetry of the helical field ripple takes place if $|\bar{\sigma}| \approx 1$. The plots of σ and $\bar{\sigma}$ against the normalized radius for various magnetic configurations (stellarators, heliotrons, torsatrons) are shown in Fig. 15(a, b). It follows from these figures that a strong vertical ripple asymmetry is inherent not only to magnetic configurations of present-day heliotrons but also to those of modular stellarators and heliacs, such as W7-AS [34] and TJ-2 [35]. The effect of side harmonics causes a change in the depth and number of secondary magnetic wells existing along the field lines and in the fraction of particles trapped into these wells. If the Fourier coefficients of these harmonics are opposite in sign and strongly differ in value, then the vertical asymmetry of magnetic field produced by satellite harmonics displays itself in the co-ordinates of local helical magnetic field extremes to be shifted along the field line in the upper half of the torus with respect to those in the lower half by $2 \sin^{-1}(\varepsilon_h \bar{\sigma} \sin \theta / \varepsilon_H)$, where $\varepsilon_h = \varepsilon_{l,1}$ and $\varepsilon_H = \left[(1 + \sigma \cos \theta)^2 + (\bar{\sigma} \sin \theta)^2 \right]^{1/2}$. With this, because of toroidicity, the depths of the secondary magnetic wells also become different near the vertical axis in the upper and lower halves of the torus, with a deeper ripple being disposed in the lower half, if $\bar{\sigma} < 0$ (the H-E case) and in the upper half, if $\bar{\sigma} > 0$. The asymmetry-caused modulation of the magnetic field strength, B/B_0 , and variations of the helical magnetic field ripple amplitude, $(B_{\max} - B_{\min})/(B_{\max} + B_{\min})$, along a field line in H-E are shown in Figs. 16(a) and 16(b), respectively [25]. Such a kind of asymmetry is local

and becomes zero if averaged over the magnetic surface. Therefore, having no effect on the orbits of those particles, which in their motion make total go-round of the torus on the minor azimuth (passing particles and passing helical bananas), the vertical asymmetry of the helical field ripple seriously affects the confinement of those high-energy particles, whose motion on the minor azimuth is essentially limited (superbananas and toroidal bananas, especially those with transient orbits). For such particles the vertical asymmetry of helical ripple wells entails a vertical asymmetry of probability of toroidal banana trapping in these wells and of delocalization of superbananas from them [26]. This can also entail a considerable vertical asymmetry of charge particle flows exhausted from the confinement volume. In heliotrons, with a large number of field periods m and $\varepsilon_h > \varepsilon_t$, where ε_h and ε_t are the helical and toroidal inhomogeneities of the magnetic field, respectively, the toroidal bananas and superbananas, as a rule, form the main fraction of lost charged particles, especially, fast ones. With this, if the drift of fast toroidal bananas from the confinement volume directed as $\mathbf{B} \times \nabla B$ for ions is not compensated by the corresponding drift of superbananas moving in the opposite direction, then in non-axisymmetric heliotrons convective flows of fast particles leaving the confinement volume will always possess some initial asymmetry caused by toroidicity. Being typical for the case of low E_r field at the periphery, a decompensation of flows of escaping toroidal bananas and superbananas in a very low collisionality regime can be eliminated for the account of a stronger electric field. The presence of vertical asymmetry of the helical field ripple can result in a considerable enhancement of the degree of vertical asymmetry for convective flows of fast particles, if the deeper helical ripple wells are positioned in the direction of the dominating particle drift from the confinement volume.

Numerical simulations of ion and electron losses in H-E show [26] that high-energy 25 keV ions leave the confinement volume mainly vertically on θ and between the helical coils on ϕ (Fig. 17) irrespective of their position on the starting magnetic surface. The $\mathbf{B} \times \nabla B$ drift of trapped toroidal banana-ions, which is directed downward in H-E, is aggravated by the helical ripple wells to be deeper in this direction than in the upward direction. This entails a considerable difference (by two orders of magnitude) between the values of escaping ion flows, which cross the LCFS in the upper and lower halves of the torus. Such a behavior of escaping fast particles qualitatively agrees with observations of large currents I_s [10,11] and positive currents I_p [14] in the divertor region in the bottom part of the torus under low heating power conditions ($P_{\text{abs}}/\bar{n}_e < 200\text{--}300 \text{ kW}/10^{19} \text{ m}^{-3}$). Accordingly, the escaping electrons, where particles barely trapped in the helical ripple wells also dominate, drift oppositely to the ion $\mathbf{B} \times \nabla B$ drift direction, i.e., upward, into the region of less deep helical ripples, where in the same conditions a comparatively small negative plasma current was recorded in the divertor region.

Studies of co-ordinate distributions of LCFS intersection by fast escaping particle orbits as functions of average radius of the starting magnetic surface show that it is mainly peripheral regions of the confinement volume, which are responsible for the vertical asymmetry of fast particle flows (Fig. 18(a, b)). For example, in H-E the asymmetry at the periphery is twice as large as in the core plasma. The same also holds for the LHD heliotron. Moreover, near the LCFS the ratio of asymmetry degrees for fast particle flows in LHD and H-E is well correlated with the parameter $\bar{\sigma}$ ratio for these configurations. Poloidal distributions of escaping particle co-ordinates on deeper surfaces in heliotrons possess a horizontal asymmetry rather than vertical one and weakly depend on $\bar{\sigma}$. This is easily explained by the fact that particles with a small poloidal rotation, toroidal bananas and superbananas, which are mostly subjected to the $\mathbf{B} \times \nabla B$ drift, usually are confined much better on the inner magnetic surfaces than on the plasma periphery, where the particle orbits of this type in a considerable extent determine the character of convective flows of fast particles.

3.2.2. Effects of magnetic axis shift

It is known that any optimization of torsatron/heliotron magnetic configuration with the purpose of particle confinement improvement, which moves the configuration closer to quasi-

symmetric one, also results in a reduction of the $\mathbf{B} \times \nabla B$ drift of charged particles and, accordingly, in a reduction of vertical asymmetry of convective flows of fast particles. One of ways to move a torsatron/heliotron configuration closer to quasi-symmetric one is creation of a configuration with the magnetic axis shifted inward with respect to the geometric minor axis of the torus [36]. An inward shift of the magnetic axis of a heliotron really results in a reduction of vertical asymmetry of fast particle flows. For example, as it has been shown in Refs. [25,26], in the standard LHD configuration with the inward 15 cm-shifted magnetic axis (LHD-IS) the value of $\bar{\sigma}$ is three times as small as in the H-E case (Fig. 15(b)), and the up-down asymmetry of fast 10 keV ions is more than order of magnitude smaller as compared with the case of outwardly shifted magnetic axis (LHD-OS, Fig. 19).

The use of additional vertical field for creation of the H-E magnetic configuration with the inwardly shifted magnetic axis resulted in a decrease of the vertical asymmetry of the diverted plasma flows, especially when an additional toroidal field (TF) was also imposed [10]. This additional field could change the rotational transform profile, the size of LCFS and the magnetic shear. As measurements have shown [10], the up-down asymmetry of diverted plasma flows vanished, when the size of LCFS was 15 % reduced under the effect of TF. The highest vertical asymmetry in H-E was observed with zero shift of the magnetic axis and without additional TF. Besides, the toroidal field in H-E was too small to create additional TF ripple wells along the field lines.

3.2.3. Effects of distant magnetic field harmonics created by additional toroidal field

It follows from comparison of fast escaping ion behavior in H-E and other vertically asymmetric stellarator-type configurations that despite the degrees of vertical helical ripple asymmetry are close at the plasma periphery for H-E and such configurations as W7-AS and TJ-2 (Fig. 15(b)), the vertical asymmetry of fast escaping ion flows is quite different in these configuration. This is explained by the presence of an additional mechanism of $\mathbf{B} \times \nabla B$ drift compensation for fast toroidal banana-ions, which, probably, exists in these configurations but is absent in H-E. An analysis of the ripple character along a field line and of escaping fast particle orbits in W7-AS shows that a partial compensation of vertically directed $\mathbf{B} \times \nabla B$ drift of toroidal bananas occurs in this configuration for the account of particles trapped into additional, third-order magnetic wells (TF ripple-trapped particles) [37] and drifting in opposite direction. Such additional magnetic wells exist along a field line in stellarator configurations with a 3D-magnetic field which is characterized by a complicated magnetic-field harmonic spectrum,

$$B/B_o = \sum_{j=0}^{\infty} \sum_{N=-\infty}^{\infty} \varepsilon_{j,N}(r) \cos(j\theta - Nm\phi),$$

where comparatively strong remote harmonics with

toroidal mode numbers $N \geq 2$ are present. Just as in tokamaks, the drifts of charged particles trapped into secondary magnetic wells and of those delocalized from these wells are directed oppositely. Therefore, the most favorable position of third-order magnetic wells, from the viewpoint of compensation of $\mathbf{B} \times \nabla B$ drift of trapped toroidal bananas from the confinement volume, is the position near local helical maxima of the magnetic field. In the case where such additional magnetic wells exist in a sufficient number, as is the W7-AS case, a considerable fraction of toroidal bananas is trapped into these wells and reverses the direction of its drift. This entails a significant reduction of the vertical asymmetry of convective flows of fast particles. For the W7-AS stellarator, the escaping fast particle distributions over pitch-angles and poloidal angles of LCFS intersection, when calculated with the total spectrum of magnetic field harmonics taken into account (Fig. 20(a)) and compared with the distributions calculated without account of remote harmonics (Fig. 20(b)), allow one to conclude that it is the remote harmonics that are responsible for the reduction of vertical asymmetry of convective particle flows in W7-AS. With this, as follows from Fig. 20, the reduction of poloidal asymmetry of fast particle flows for the account of additional ripple is accompanied in such configurations by a rise of lost particle orbit spread in the velocity space too.

This is an indication that an additional group of particles occurs in the convective flow, with the type of orbits differing from that of toroidal bananas.

It follows from the comparison of experimental data for divertor flow distributions and numerical calculations of particle losses for TJ-2 ($l = 1$), H-E and LHD ($l = 2$), U-3M ($l = 3$) and W7-AS (a multiple- l system) that the degree of vertical asymmetry of fast particle loss, which presumably results in vertical asymmetry of divertor flows, decreases with l , in general, even if the configuration is not drift-optimized.

3.3. Possible impact of E_r on particle losses and divertor flow asymmetry in H-E

NBI usually results in occurrence of a negative potential $e\Phi/T \sim -(1-2)$ in the confinement volume (“ion root” [27]) and a negative radial electric field E_r , whose strength could attain ~ 100 V/cm in H-E [38]. The mechanisms having been considered in Sec. 3.2 give a qualitatively correct explanation of the vertical asymmetry of divertor flows, which was observed in H-E under comparatively low heating power conditions ($P_{\text{abs}}/\bar{n}_e < 200\text{--}300 \text{ kW}/10^{19} \text{ m}^{-3}$), where the effect of E_r on the orbits of fast charged particles arising from NBI was small ($\Omega_{VB} \gg \Omega_{EXB}$). With the increase of heating power for the account of summed flux of injected neutrals rise, the fast ion losses also rose. As follows from calculations and measurements [38–41], the fast ion losses and charge exchange seriously affect the value of electric field and its profile. Owing to the losses, the resultant electric field usually becomes more negative. Facilitating improvement of thermal ion confinement due to delocalization of majority of ions from the helical ripple wells, such an electric field is still small to provide a complete confinement of fast toroidal banana-ions, and a part of these particles continues to drift vertically downward. With occurrence of helical resonance $\Omega_{VB} + \Omega_{EXB} \approx 0$ for the fast ions, a considerable part of them can turn into superbananas and be lost from the confinement volume, drifting vertically upward, while the fraction of escaping toroidal bananas drifting downward is considerably reduced. Thus, beginning with a certain heating power, the degree of vertical asymmetry of convective flows of lost fast particles decreases under the influence of E_r profile modification at the periphery.

A negative electric field usually deteriorates fast electron confinement. As the heating power increases, the toroidal resonance condition, $\Omega_T + \Omega_{EXB} \approx 0$, for fast electrons begins to be fulfilled, facilitating transition of more and more electrons into toroidal bananas. The losses of this group of particles drifting vertically upward dominate among the electrons. A situation is possible, where the convective flows of ions and electrons drifting in the same direction coincide, and this will result in a considerable reduction of the vertical asymmetry of ambipolar divertor flows (cf. the Fig. 9(a) plots at $P_{\text{abs}}/\bar{n}_e \approx 200\text{--}300 \text{ kW}/10^{19} \text{ m}^{-3}$).

As follows from Fig. 9(a), with a further increase of normalized heating power ($P_{\text{abs}}/\bar{n}_e > 200\text{--}300 \text{ kW}/10^{19} \text{ m}^{-3}$), the plasma current reverses its direction in the inner divertor legs at the top and bottom of the ($0^\circ/m$) cross-section. To explain this effect, other mechanisms of particle loss should be put into consideration. The radial electric field shear dE_r/dr could be one of the factors affecting the plasma current direction. The role of this factor in plasma confinement is mentioned in Refs. [31, 39–41]. It is known [38] that with the electric field shear being high enough in a tokamak, a so-called “drift reversal” for the trapped particles occurs. If such an effect occurred in H-E, then the fast toroidal banana-electrons would leave the confinement volume mainly in the lower part of the torus, this being in a qualitative agreement with a large negative plasma current to be picked up by the bottom collecting plates at a high heating power [14].

As it has been shown in Ref. [41], with ECH imposed on NBI, the field E_r tends to become more positive ($\Delta E_r > 0$). This regime is characterized by the points $\blacktriangle, \blacklozenge$ in the lower part of Fig. 9(a). A positive electric field and $\Phi > 0$ are also characteristic of ECH-only to be used for plasma heating [43] (“electron root” [27]). It is known [44] that a positive electric field gives rise to a reduction of the ion loss cone. In these conditions, a major part of fast ions turns into well confined deeply trapped particles, and the fast electrons are a dominating type of escaping particles

during ECH. With the presence of positive electric field, the helical resonance condition can be fulfilled for these particles, this resulting in their conversion into superbananas and vertical drift to the lower part of the torus. Such a process would also be in a qualitative agreement with observations of large negative plasma currents in the lower part of the torus in H-E.

In the additional ECH-1 case, since a considerable fraction of microwave power was deposited at the periphery, we may expect that the field E_r changing at the periphery, in the first place, affected the orbits of trapped fast ions more efficiently than in the additional ECH-2 case [40]. Moreover, as is stated in Ref. [41], with ECH-2 imposed on NBI, an additional heating of ions and improvement of their confinement could be compensated by the “pump-out” and density flattening effects. Possibly, this is why fast changes of I_s and I_p were not observed with the additional ECH-2 switched on.

Thus, basing on available information, which concerns a possible effect of the radial electric field on fast particle orbits in helical devices, we can set a qualitative link, with a certain degree of authenticity, between fast particle losses and the distributions of ambipolar and non-ambipolar flows of diverted plasma, in particular, vertical asymmetry of these distributions in H-E. However, the available experimental database is not sufficient to make more definite conclusions. Special additional studies are necessary, including numerical modeling of fast particle dynamics in both the confinement volume and the divertor layer with the field E_r , its profile taken into account.

3.4. Predictions of fast particle behavior in the SOL region: effects of magnetic field parameters and heating conditions

As calculations have shown [45,46], for alpha particles, whose orbits are insensitive to collisions and electric field effects, the distance between the LCFS and the vacuum vessel is the main parameter, affecting the behavior of these particles in the SOL region of an $l=2$ helical device. In these calculations, with B_ϕ directed counterclockwise, the escaping alpha particles form a vertically asymmetric narrow strip on the LCFS, which closely follows the path of one of the X-points on the inner and upper torus side ($\pi/2 < \theta < \pi$). If the distance between the LCFS and the first wall is comparatively small, then the escaping alpha particles crossing the LCFS move directly to the first wall, being also strongly focused on the above mentioned strip [46]. Such a behavior of alpha particles does not depend on the aspect ratio of the configuration and the number of magnetic field periods. If the distance between the LCFS and the first wall is large enough, then those alpha particles, which cross the LCFS near the X-point on the inner torus side can be reflected, cross the X-point private region and reach the other separatrix leg. These particles are confined in the SOL region, bouncing from one to another separatrix leg. Calculations carried out for the LHD case [47] have shown that the behavior of particles trapped between two X-points could also be of stochastic character due to field line stochastization outside the separatrix. Since a stochastic layer outside the LCFS is inherent to all helical magnetic configurations, the above mentioned behavior of particles in SOL is predicted to be typical for all torsatrons and heliotrons. Another group of escaping alpha particles, i.e. those crossing the LCFS near the vertical plane, will be lost, because the distance between LCFS and the wall is insufficiently large to confine these particles in SOL. Probably, the distance between the plasma boundary and first wall required to confine particles in SOL depends on the fraction of particles with the vertical direction of the drift crossing a LCFS. The larger this fraction is, the larger distance is necessary. Therefore, in drift-optimized torsatron/heliotron configurations, where the fraction of particles with the vertical drift is decreased considerably, it is possible to confine in SOL all particles crossing the LCFS, if the distance between LCFS and the vacuum vessel is sufficiently large.

The behavior in the SOL region of fast particles with lower energies, such as the injected particles, is affected by electric fields and collisional transport, which depend on the heating conditions and edge temperature. All these processes strongly influence the heat load in the divertor region. As it is shown in Ref. [24], in a tokamak with a single-null divertor, for high edge temperature conditions when the heat load in the divertor region is caused mainly by a fast ion flux

from the plasma volume, three spots of intense heat deposition in the divertor region can be observed. Two of these spots correspond to fast trapped ions and are located on the high field side. One of them, located near the vertical plane, is caused by escaping trapped fast ions drifting across the field lines. Another spot on the high field side is caused by passing ions moving along the separatrix leg away from the X-point. The third spot is located on the low field side and corresponds to passing electrons moving away from the X-point along another separatrix leg. In the lower temperature conditions when drift effects are unimportant, the behavior of heat deposition spots is mainly determined by passing particles from SOL, producing two hot spots located near two legs of the X-point, one of them from ions and one from electrons [24]. A similar behavior of heat deposition spots is typical for the drift-optimized configuration case when the contribution from trapped ions vanishes [24].

Basing on this information, though quite scarce one, besides of vertical asymmetry, a considerable spread of particle flows, in particular, for the account of fast particle outflow, should be expected in the divertor region of a heliotron/torsatron as compared with the spatial distribution of main divertor magnetic fluxes.

4. Summary

Experimental studies of poloidal distributions of diverted plasma flows in the $l=2$ Heliotron E heliotron and $l=3$ Uragan-3M torsatron have been carried out. A strong vertical asymmetry of these distributions has been revealed as a result of these studies. The main investigations in Heliotron E were carried out with one direction of the toroidal magnetic field. However, various methods of plasma heating were used (NBI, fundamental and second harmonic ECH, NBI+ECH). All investigations in Uragan-3M were performed with a fixed regime of RF plasma production and heating. However, both directions of the toroidal magnetic field were examined. A joint analysis of experimental results obtained on two devices differing in their magnetic configuration and plasma parameters in combination with results of theoretical analysis and numerical modeling of non-diffusive charged particle losses in stellarator-type devices allows one to make some conclusions concerning characteristics of the asymmetry and its nature.

1. A many-fold difference has been observed in the values of ambipolar plasma flows when estimating these values by the ion saturation current I_s to Langmuir probes (collecting plates) installed symmetrically about the midplane in the divertor region in the top and bottom parts of the torus. This difference increased with the distance from the midplane and attained ~ 50 times in Heliotron E and ~ 3 times in Uragan-3M.

2. In non-ambipolar plasma flows characterized by the value and sign of the current I_p to a grounded Langmuir probe (collecting plate), particles with opposite signs dominated in the upper and lower parts of the divertor region. In Uragan-3M, a non-ambipolar flow with an excess of ions ($I_p > 0$) corresponded to the larger ambipolar flow. A similar correspondence took place in Heliotron E at a lower heating power ($P_{\text{abs}}/\bar{n}_e < 200\text{--}300 \text{ kW}/10^{19} \text{ m}^{-3}$). At a higher heating power, a non-ambipolar flow with an excess of electrons ($I_p < 0$) corresponded to the larger ambipolar flow.

3. In Uragan-3M and in Heliotron E with a lower heating power, the dominating direction of diverted plasma outflow coincided with the ion toroidal $\mathbf{B} \times \nabla B$ drift direction. The leading role of the toroidal $\mathbf{B} \times \nabla B$ drift in formation of vertical asymmetry of divertor flows under these conditions was confirmed by asymmetry reversal with reversal of the toroidal magnetic field direction in Uragan-3M.

4. The leading role of the toroidal $\mathbf{B} \times \nabla B$ drift in asymmetry formation means that the direct (non-diffusive) losses of charged particles from the confinement volume had a determinative effect on the divertor flow distribution in Heliotron E and Uragan-3M. In a numerical modeling of direct particle losses in Uragan-3M and in Heliotron E with a low heating power a qualitative agreement has been obtained between the angular distributions of lost particle orbits and the directions of

dominating electron and ion outflows into the divertor region. A contribution of convective losses to the formation of diverted plasma flows, their asymmetry in the Heliotron E case was also evidenced by fast variations of the currents I_s , I_p and potential V_f , which were observed with a fast heating power rise. Besides with their direct outflow to the divertor region, the fast ions and electrons, when drifting into different regions of the edge plasma, must result in an inhomogeneous poloidal distribution of the potential in this plasma and in induction of electric currents (plasma currents) of different signs in corresponding regions of the SOL and diverted plasmas. Not only fast particles but also thermal ones diffusing from the confinement volume will participate in such a transport.

5. Proceeding from the character of $I_s/\bar{n}_e - P_{\text{abs}}/\bar{n}_e$ plots for Heliotron E, we may suppose that a significant vertical asymmetry of divertor flows was present in this device even in the limit of zero heating power. Such an initial asymmetry could result from minor distortions of the real divertor magnetic configuration due to a displacement or deformation of the magnetic coils. The heating of the plasma in Heliotron E gave rise to a modification of the asymmetry and its further increase.

6. Being supposedly responsible in a great extent for the asymmetry in divertor flow distributions, the toroidal $\mathbf{B} \times \nabla B$ drift-caused vertical asymmetry in fast particle loss distributions is multiply enhanced in Heliotron E due to the natural vertical asymmetry of the helical magnetic field ripple, which is inherent to all $l = 2$ torsatrons/heliotrons and to other stellarator-type configurations and is a manifestation of deviation of these configurations from quasi-helical symmetry.

7. Any optimization of a torsatron/heliotron magnetic configuration with the purpose of confinement improvement, which approaches the configuration to the quasi-helical symmetry, also results in a reduction of the toroidal $\mathbf{B} \times \nabla B$ drift of charged particles and, consequently, in a reduction of vertical asymmetry of convective flows of fast particles. Accordingly, a reduction of the vertical asymmetry of diverted plasma flows should be expected. A creation of configuration with the inwardly shifted magnetic axis with respect to the minor geometric axis of the torus is one of the ways to approach a torsatron/heliotron configuration to symmetric one. Another way to compensate the vertical asymmetry of secondary magnetic wells and the toroidal $\mathbf{B} \times \nabla B$ drift-caused vertical asymmetry of lost particle flows in a stellarator is a creation of magnetic wells with a multi-rippled structure along the field lines.

8. It follows from the comparison of experimental data for divertor flow distributions and numerical calculations of particle losses for TJ-2 ($l = 1$), H-E and LHD ($l = 2$), U-3M ($l = 3$) and W7-AS (a multiple- l system) that the degree of vertical asymmetry of fast particle loss, which presumably results in vertical asymmetry of divertor flows, decreases with l , in general, even if the configuration is not drift-optimized.

9. As calculations have shown, the account of the radial electric field E_r in Uragan-3M (up to 40 V/cm in absolute value) does not result in qualitative changes in the character of distributions of convective flows of lost electrons and ions in the lower and upper halves of the torus. In Heliotron E the field E_r could attain -100 V/cm, its value and sign depending on the absorbed power and the method of heating. The reversal of sign of dominating particle charge in the non-ambipolar divertor flows at the top and bottom with the increase of heating power could be an indication of reversal of convective flows of escaping particles. This results from change in the type of dominating escaped particles (electrons or ions). In principle, this reversal could be related to strong distortions of the fast electron and ion orbits affected by heating-caused changes in the value of the field E_r , its sign and profile.

Proceeding from what have been presented above, experimental, analytic and numerical studies of the effect of direct particle losses on the electric field structure in the edge plasma and of the impact of this field on thermal and fast particle transport in the edge and diverted plasma should become a highly important part of divertor research.

Acknowledgements

This work was in part carried out within the Agreement on Scientific Collaboration between IPP NSC KIPT (Kharkov) and IAE, Kyoto University (Japan) and within the LIME Program (NIFS, Japan).

References

- [1] Wagner, F., Keilhacker, M. and the ASDEX and NI Teams, J. Nucl. Mater. **121** (1984) 103.
- [2] Maeda, H., et al., Nucl. Fusion **16** (1976) 148.
- [3] Bonnin, X., Rowan, W.L., Nucl. Fusion **39** (1999) 1009.
- [4] Hutchinson, I.H., et al., Plasma Phys. Control. Fusion **37** (1995) 1389.
- [5] Yamamoto, S., et al., Nucl. Fusion **18**(2) (1978) 205.
- [6] Marchand, R., et al., Nucl. Fusion **35** (1995) 297.
- [7] Ohyabu, N., et al., Nucl. Fusion **34** (1994) 387.
- [8] Noda, N., et al., J. Plasma Fusion Res. SERIES **3** (2000) 180.
- [9] Mizuuchi, T., et al., in Controlled Fusion and Plasma Physics (Proc. 18th Eur. Conf. Berlin, 1991), Vol. 5C, Part III, EPS, Geneva (1991) 65.
- [10] Mizuuchi, T., et al., J. Nucl. Mater. **266-269** (1999) 1139.
- [11] Chechkin, V.V., et al., Nucl. Fusion **40** (2000) 785.
- [12] Chechkin, V.V., et al., Plasma flow asymmetries in the natural helical divertor of an $l = 3$ torsatron and their relation to particle losses, Nucl. Fusion (submitted).
- [13] Pitcher, C.S. and Stangeby, P.C., Plasma Phys. Control. Fusion **39** (1997) 779.
- [14] Chechkin, V., et al., J. Plasma Fusion Res. SERIES **3** (2000) 197.
- [15] Mizuuchi, T., et al., J. Nucl. Mater. **162-164** (1989) 105.
- [16] La Haye, R.J., Nuclear Fusion **31** (1991) 1550.
- [17] Volkov, E.D., et al., in Controlled Fusion and Plasma Physics (Proc. 23rd EPS Conf. Kiev, 1996), Vol. 20C, Part II, EPS, Geneva (1996) 571.
- [18] Bykov, V.Ye., et al., in Stellarators and Other Helical Confinement Systems (Collection of papers presented at the IAEA Technical Committee Meeting, Garching, Germany, 1993), IAEA, Vienna (1993) 391.
- [19] Bykov, V.Ye., et al., Plasma Phys. Control. Fusion **37** (1995) 271.
- [20] Chechkin, V.V., et al., Nucl. Fusion **36** (1996) 133.
- [21] Maassberg, H., et al., Plasma Phys. Control. Fusion **35** (1993) B319.
- [22] Mizuuchi, T., et al., in Controlled Fusion and Plasma Physics (Proc. 23rd Eur. Conf. Kiev, 1996), Vol. 20C, Part II, EPS, Geneva (1996) 507.
- [23] Gurevich, A. V., Dimant, Ya. S., Kinetic theory of fast particle transport in tokamaks, in Reviews of Plasma Physics, Vol. 16 (Kadomtsev, B.B., Ed.), Consultants Bureau, New York (1990) 3.
- [24] Core, W.G.F., Lazzaro, E., Phys. Fluids B **5** (1993) 1173.
- [25] Smirnova, M.S., Phys. Plasmas **5** (1998) 3986.
- [26] Smirnova, M.S., Phys. Plasmas **6** (1999) 897.
- [27] Rome, J.A., Nucl. Fusion **35** (1995) 195.
- [28] Skibenko, A.I., et al., Ukrainian Journal of Physics **46** (2001) 443.
- [29] Hanatani, K., et al., Nucl. Fusion **25** (1985) 259.
- [30] Hanatani, K., Penningsfeld, F.-P., Nucl. Fusion **32** (1992) 1769.
- [31] Itoh, K., Itoh, S.-I., Plasma Phys. Control. Fusion **38** (1996) 1.
- [32] Hanatani, K., Wakatani, M. and Uo, K., Nucl. Fusion **21** (1981) 1067.
- [33] Yushmanov, P.N., Cary, J.R., Shasharina, S.G., Nucl. Fusion **33** (1993) 1293.
- [34] Stroth, U., et al., Plasma Phys. Control. Fusion **40** (1998) 1551.
- [35] Alejandre, C., et al., Fusion Technol. **17** (1990) 131.
- [36] Todoroki, J., J. Phys. Soc. Jpn. **59** (1990) 2758.

- [37] Smirnova, M.S., Phys. Plasmas **3** (1996) 2961.
- [38] Ida, K., et al., Phys. Rev. Lett. **76** (1966) 1268.
- [39] Sanuki, H., et al., J. Phys. Soc. Jpn. **60** (1991) 3698.
- [40] Ida, K., et al., Plasma Phys. Control. Fusion **38** (1996) 1433.
- [41] Obiki, T., et al., in Fusion Energy 1996 (Proc. 16th IAEA Conf. Montreal, 1996), Vol. 2, IAEA, Vienna (1997) 13.
- [42] Ida, K., et al., in Fusion Energy 1996 (Proc. 16th IAEA Conf. Montreal, 1996), Vol. 2, IAEA, Vienna (1997) 151.
- [43] Obiki, T., et al., in Plasma Physics and Controlled Nuclear Fusion Research 1988 (Proc. 12th IAEA Conf. Nice, 1988), Vol. 2, IAEA, Vienna (1989) 337.
- [44] Uo, K., Nakasuga, M., Nucl. Fusion **28** (1982) 1386.
- [45] Alladio, F., Batistoni, P., Mancuso, A., Fusion Technol. **22** (1992) 474.
- [46] Alladio, F., Batistoni, P., Mancuso, A., in Stellarators and Other Helical Confinement Systems (Collection of papers presented at the IAEA Technical Committee Meeting, Garching, Germany, 1993), IAEA, Vienna (1993) 363.
- [47] Watanabe, T., Ishida, A., Hatori, T., Kakuyugo Kenkyu **68** (1992) 298.

Figure captions

Fig. 1. Heliotron E. Symmetric poloidal cross-sections ($0^\circ/m$) and ($90^\circ/m$), where $m=19$. Shown are: positions of the helical coils, vacuum chamber, arrays of collecting plates with plate numbers $N = 1, 2, \dots, 7$, and Poincare plots of the field lines of the edge magnetic structure.

Fig. 2. Uragan-3M. Symmetric poloidal cross-sections A-A ($\phi = 0^\circ$) and D-D ($\phi = 20^\circ$) of the torus. Shown are: helical coil casings I, II, III; Langmuir probe arrays with probe numbers $N = 1-17$, 1-15, 1-6 (A-A) and $N = 1-9$, 1-23, 1-8 (D-D); Poincare plots of field lines of the edge magnetic structure.

Fig. 3. Heliotron E. Ion saturation current distribution over collecting plates $I_s(N)$ (shaded rectangles); NBI, $P_{inj} \approx 0.7$ MW, $\bar{n}_e \approx 1.7 \times 10^{19} \text{ m}^{-3}$. Calculated connection length L as a function of poloidal angle θ (solid lines) for open field lines, with the starting points lying on the lines of collecting plate array disposition in the top and bottom spacings of the cross-section ($0^\circ/m$) and in the outboard spacing of the cross-section ($90^\circ/m$). Positions of collecting plates $N = 1, 2, \dots, 7$ are indicated by bold segments.

Fig. 4. Uragan-3M. Ion saturation current I_s as a function of probe number N in the top and bottom spacings of the cross-section A-A and in the outboard spacing of the cross-section D-D. Left column, negative magnetic field; right column, positive magnetic field.

Fig. 5. Heliotron E. Current to a grounded collecting plate distribution over collecting plates $I_p(N)$ (shaded rectangles) in the top and bottom spacings of the cross-section ($0^\circ/m$) and in the outboard spacing of the cross-section ($90^\circ/m$). NBI, $P_{inj} \approx 0.7$ MW, $\bar{n}_e \approx 1.7 \times 10^{19} \text{ m}^{-3}$.

Fig. 6. Uragan-3M. Same as in Fig. 4 for the current to a grounded probe I_p .

Fig. 7. Heliotron E. Density-normalized ion saturation current I_s/\bar{n}_e as a function of density-normalized absorbed power P_{abs}/\bar{n}_e in the inner divertor legs ($N = 5$) in the top and bottom spacings of the cross-section ($0^\circ/m$) for various regimes of plasma heating: NBI (\bullet), ECH-1 (\circ), ECH-2 (\square), NBI+ECH-1 (\oplus), NBI+ECH-2 (\boxplus), NBI+ECH-1+ECH-2 (\boxtimes). The interpolating straight lines are drawn through the NBI-only points. The insets show time traces of current I_s increment induced by a 25 ms ECH-1 pulse imposed on NBI.

Fig. 8. Heliotron E. Same as in Fig. 7 for the outboard spacing of the cross-section ($90^\circ/m$).

Fig. 9. Heliotron E. (a) Density-normalized current to a grounded collecting plate I_p/\bar{n}_e as a function of density-normalized absorbed power P_{abs}/\bar{n}_e in the inner divertor legs ($N = 5$) in the top (open points) and bottom (solid points) spacings of the cross-section ($0^\circ/m$). \circ, \bullet - NBI; $\triangle, \blacktriangle$ - NBI+ECH-1; \diamond, \blacklozenge - NBI+ECH-1+ECH-2. (b) Density \bar{n}_e together with the time sequence of initial ECH, long NBI and additional ECH-1 and NBI pulses imposed on the long NBI; current I_p to the plate $N = 5$ at the bottom.

Fig. 10. Heliotron E. Same as in Fig. 9(a) for the outboard spacing of the cross-section ($180^\circ/m$) ($N = 2, 6$).

Fig. 11. Heliotron E. Floating potential V_f response to additional NBI (left column) and ECH-1 (right column) pulses imposed on a long NBI in the inner divertor legs at the top and bottom of the cross-section ($0^\circ/m$) ($N = 5$) and for divertor legs in the outboard spacing of the cross-section ($180^\circ/m$) ($N = 2, 5$).

Fig. 12. Uragan-3M. Typical trajectories of escaping test particles, 1.2 keV electrons (a) and 0.5 keV ions (b), in Cartesian coordinates in projection on the $\phi = 0$ plane for the negative magnetic field case. The major axis of the torus is on the left. The last closed magnetic surface ($r/\bar{a} = 1$) is drawn by a solid bold line.

Fig. 13. Uragan-3M. Angular coordinates of trajectories of escaping test particles, 1.2 keV electrons (a) and 0.5 keV ions (b) on the last closed magnetic surface for the cases of negative (open circles) and positive (closed circles) magnetic field.

Fig. 14. Uragan-3M. Distribution of escaping test particles, 1.2 keV electrons (a) and 0.5 keV ions (b), in the poloidal coordinate of particle orbit intersection of the last closed magnetic surface for the negative (solid lines) and positive (dashed lines) magnetic field cases.

Fig. 15. Parameters of magnetic configuration asymmetry σ and $\bar{\sigma}$ as functions of the normalized average radius of the magnetic surface r/\bar{a} for various stellarator-type configurations: W7-AS (\square), LHD (\bullet), H-E ($+$), H-J (\triangle) и TJ-2 (\circ).

Fig. 16. Heliotron E. Magnetic field strength modulation (a) and helical ripple amplitude variation along a field line (b) as functions of poloidal angle θ . $r/\bar{a} = 0.7$. The number of field line transits around the torus is 2.

Fig. 17. Heliotron E. Footprints of lost test 25 keV ions (a) and electrons (b) depending on toroidal and poloidal coordinates of trajectory position on the starting magnetic surface $r/\bar{a} = 0.7$ (open circles) and on the last closed magnetic surface $r/\bar{a} = 1$ (solid circles).

Fig. 18. Distribution functions in poloidal coordinates of lost fast ion orbits on the last closed magnetic surface in Heliotron E (total particle energy is 25 keV) and Large Helical Device (100 keV) with various values of the normalized average radius of the starting magnetic surface r/\bar{a} as parameter.

Fig. 19. Large Helical Device. Distribution functions of poloidal coordinates of lost 10 keV ion orbits in the standard LHD configurations with the inward (LHD-IS, solid line) and outward (LHD-OS, dashed line) shift of the magnetic axis.

Fig. 20. Wendelstein 7-AS. Distribution functions of lost 10 keV ions in poloidal angle θ and pitch-value V_{\parallel}/V taken at the moment of last closed magnetic surface intersection (configuration W7-AS3Z2, $\iota = 0.3$): (a) with account of total magnetic field harmonic spectrum in the calculations of charged particle losses; (b) without account of remote harmonics with toroidal mode numbers $N \geq 2$.

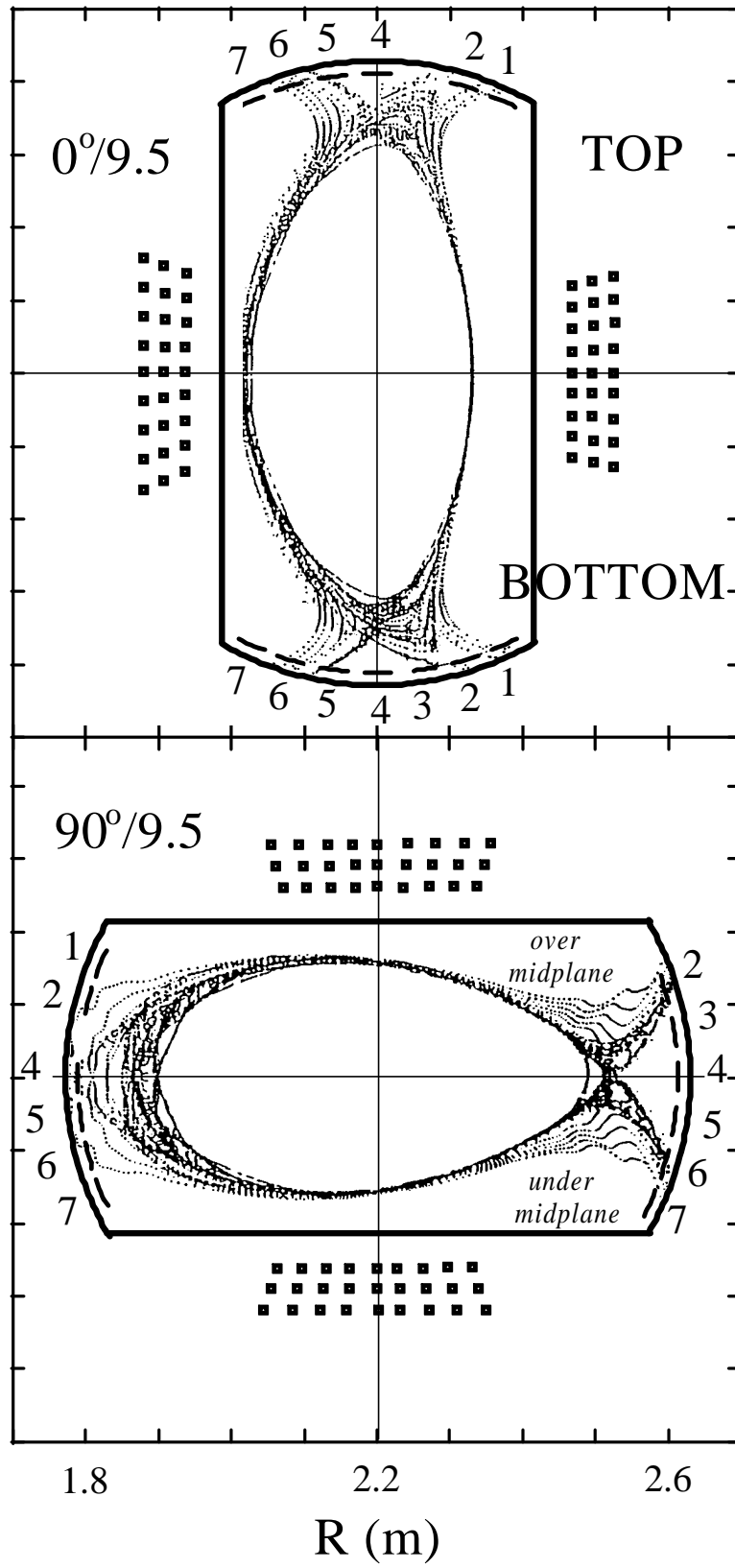


Fig. 1

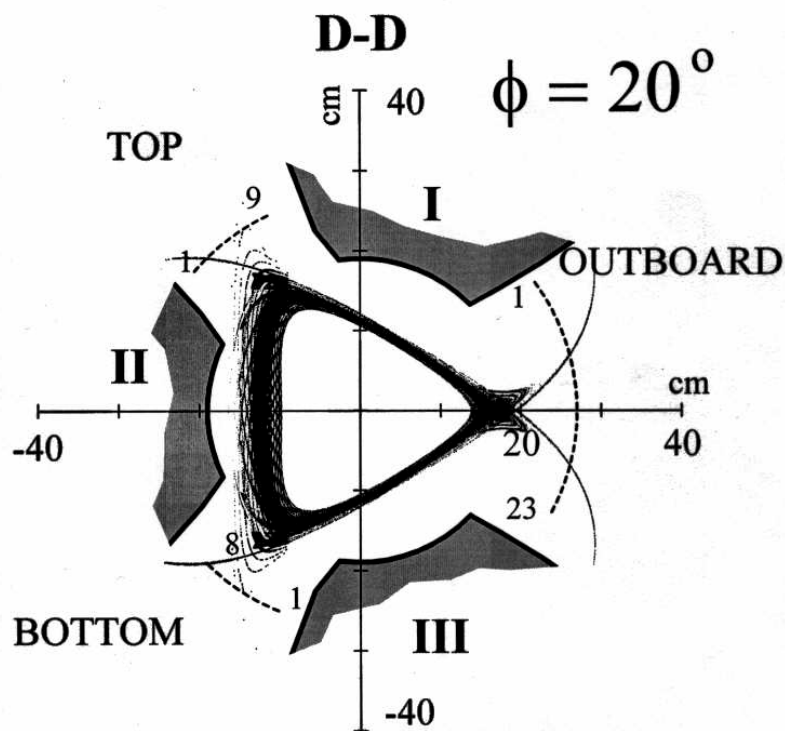
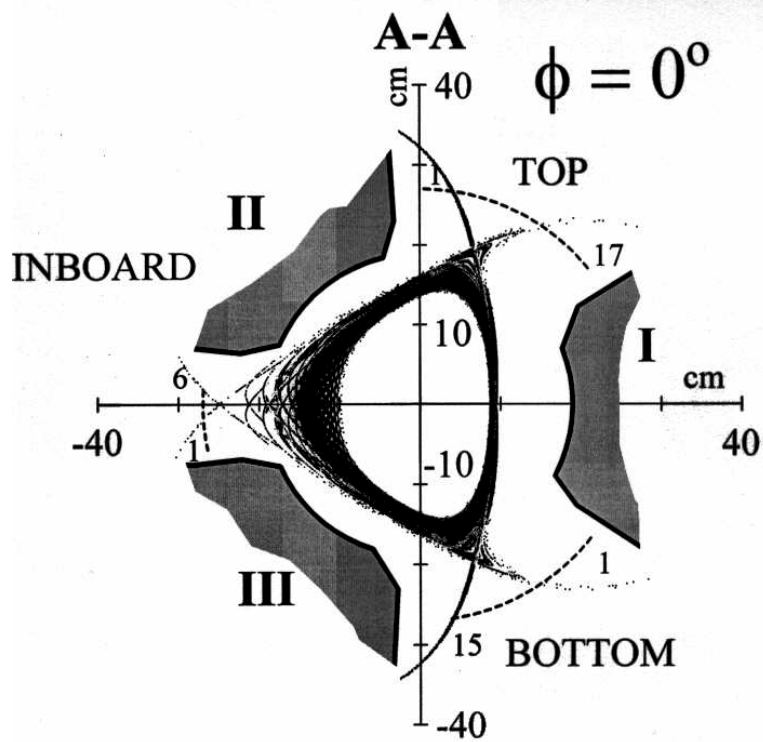


Fig. 2

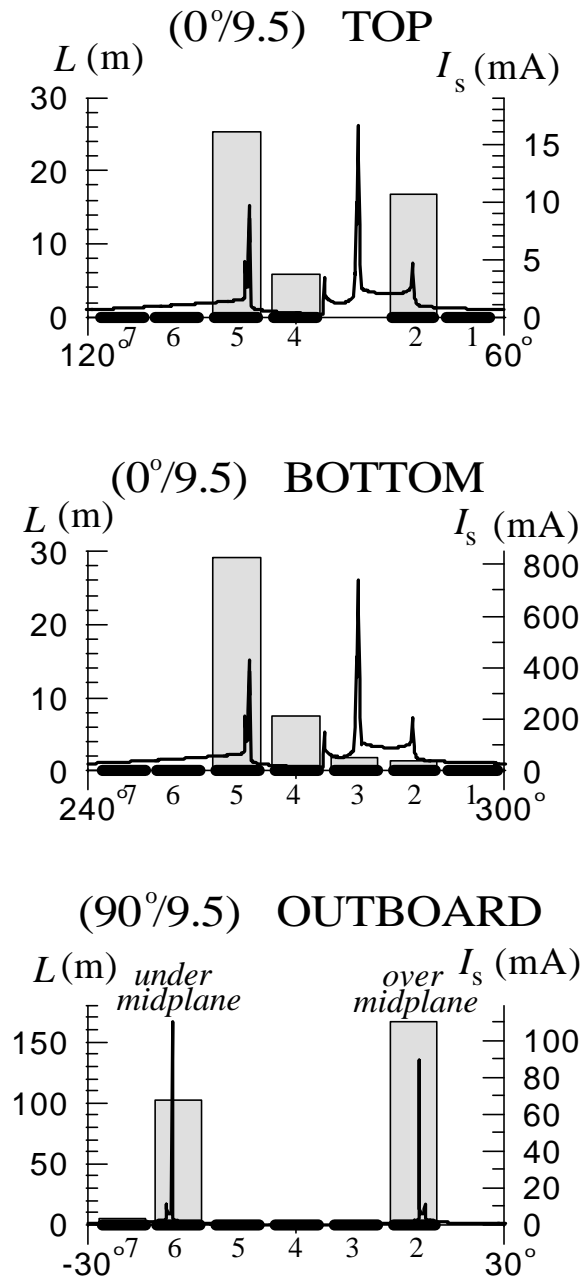


Fig. 3

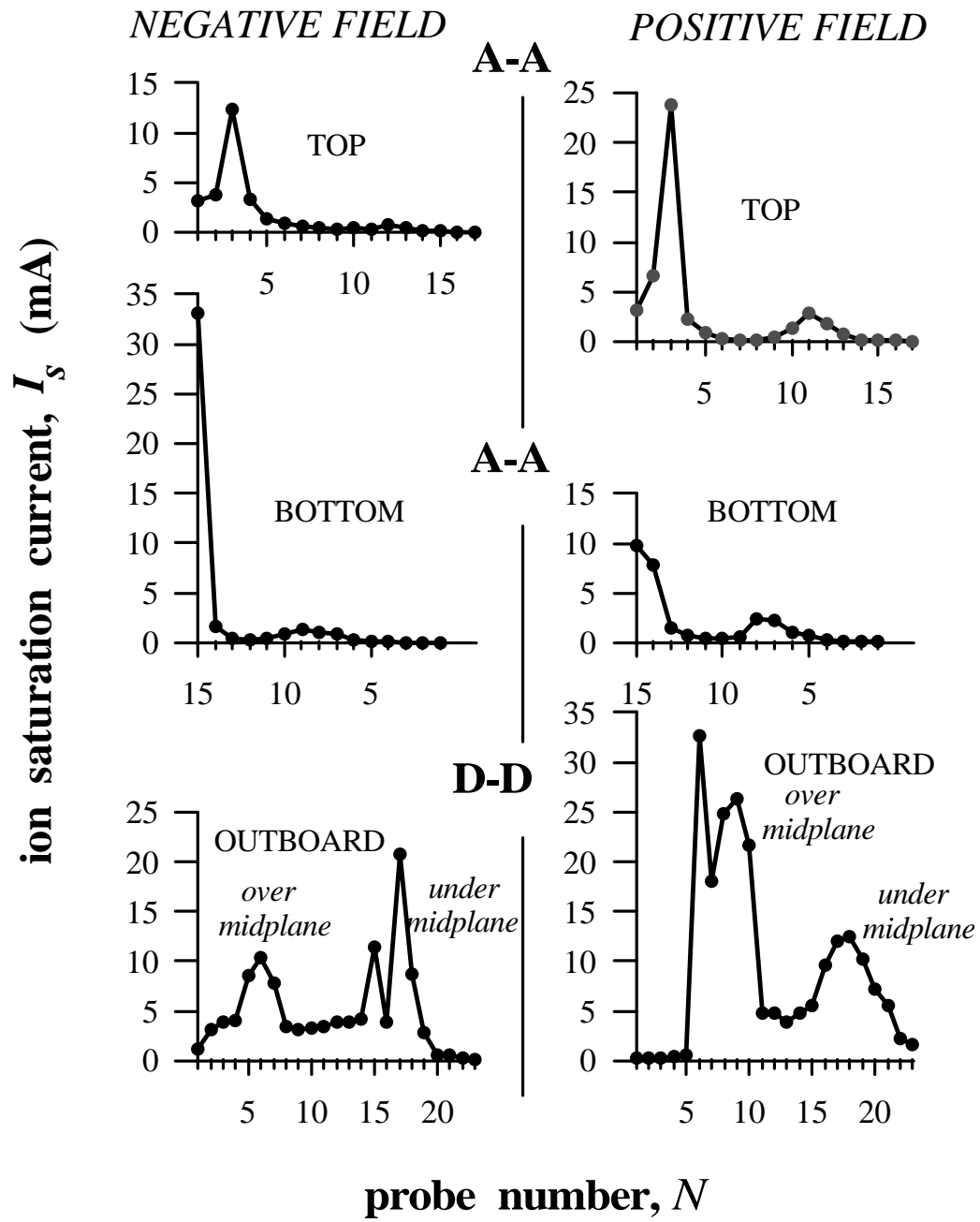


Fig. 4

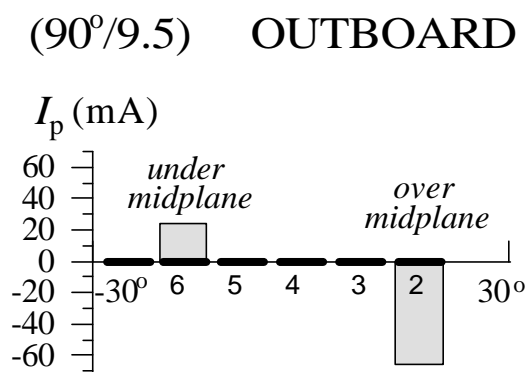
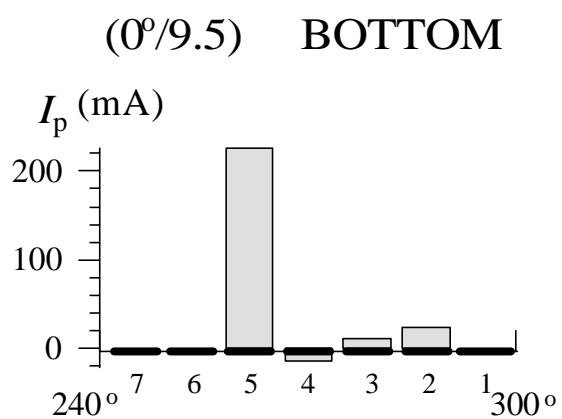
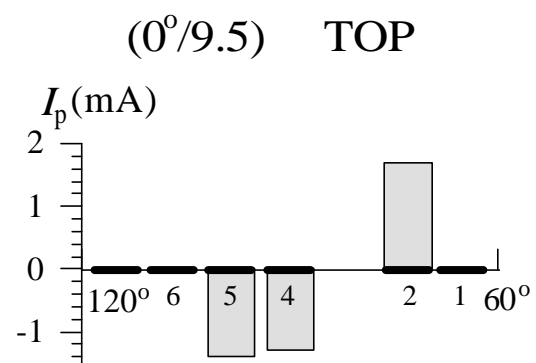


Fig. 5

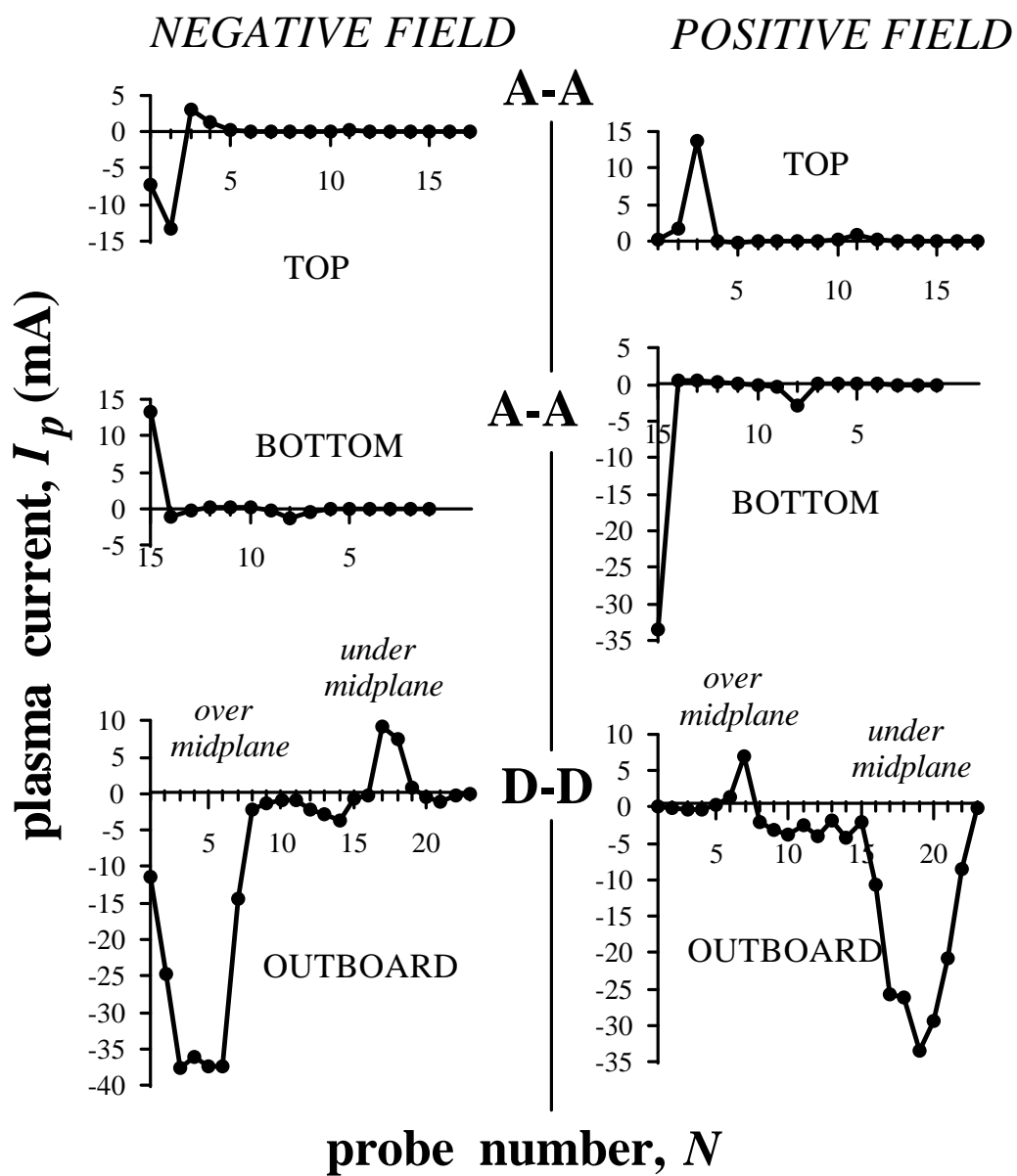


Fig. 6

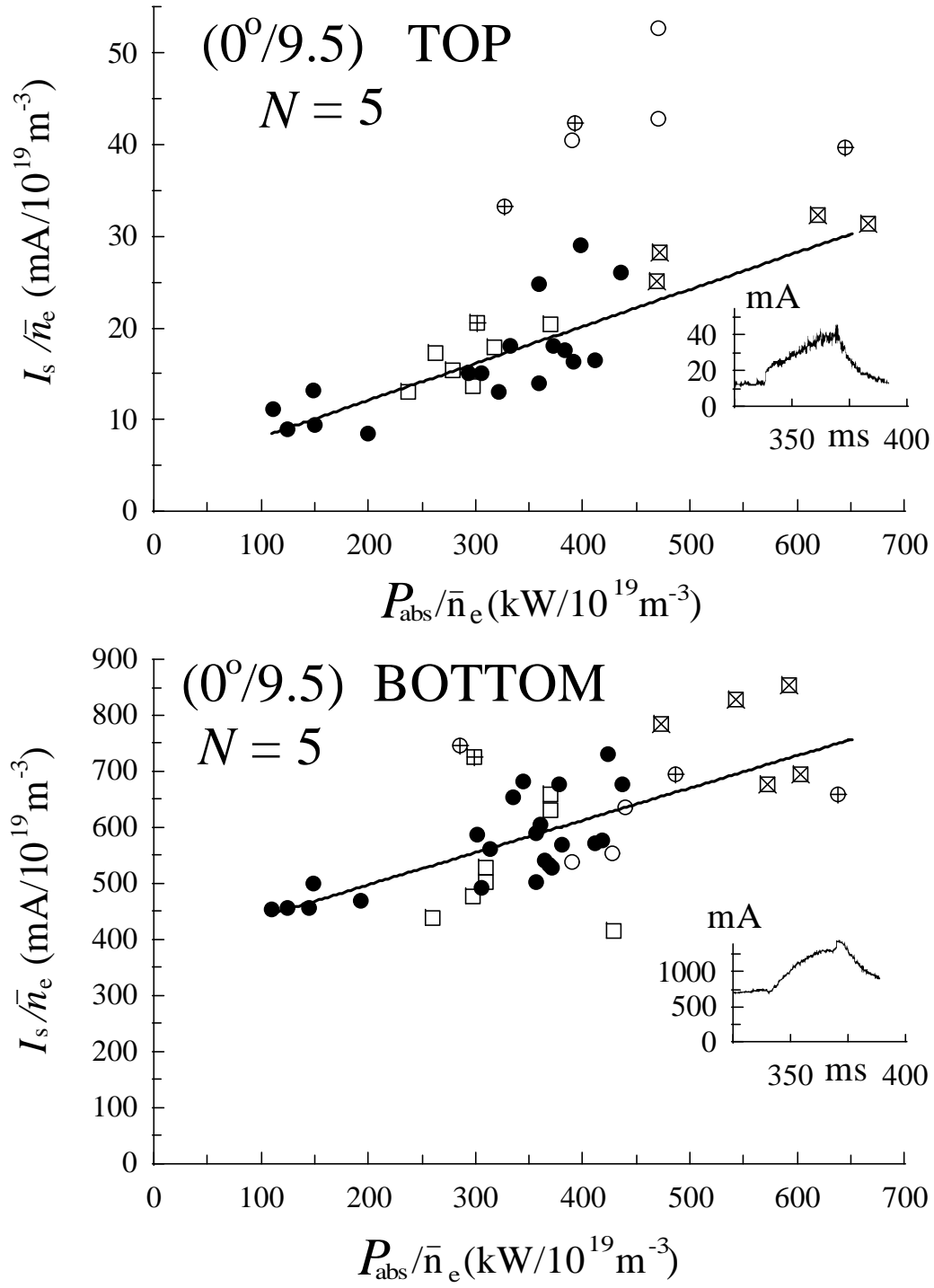


Fig. 7

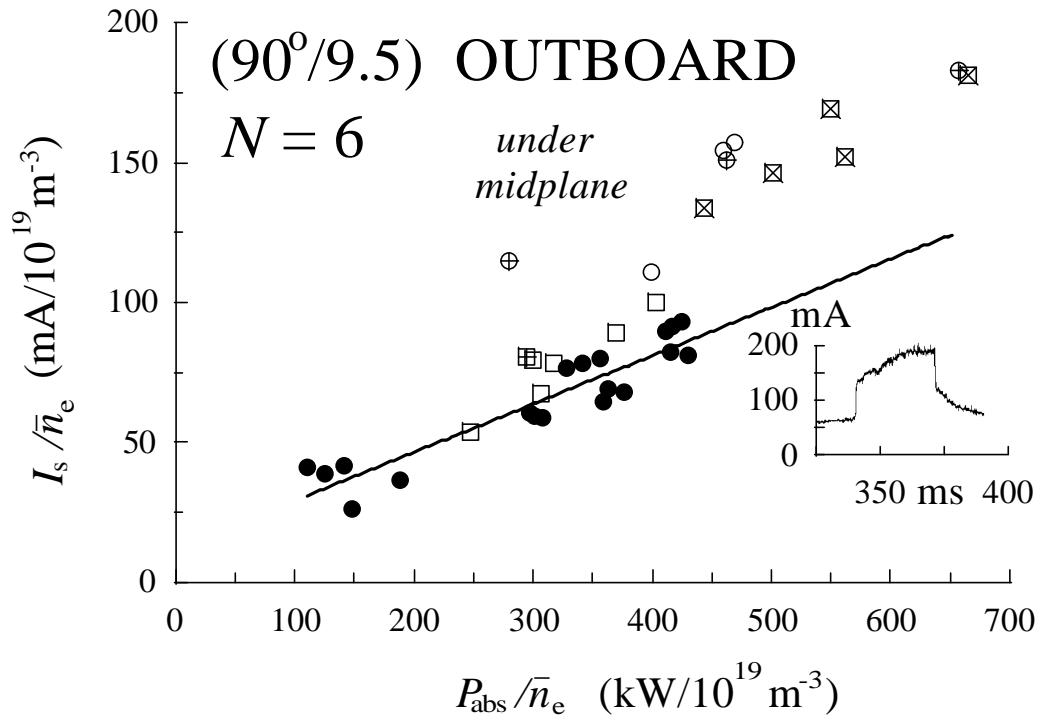
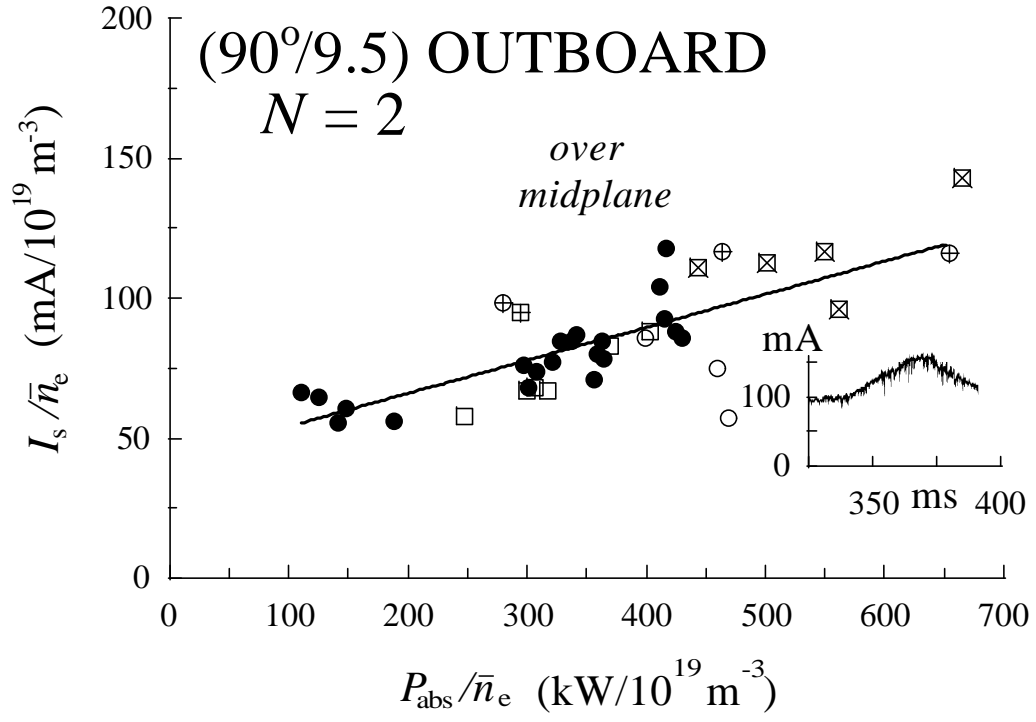
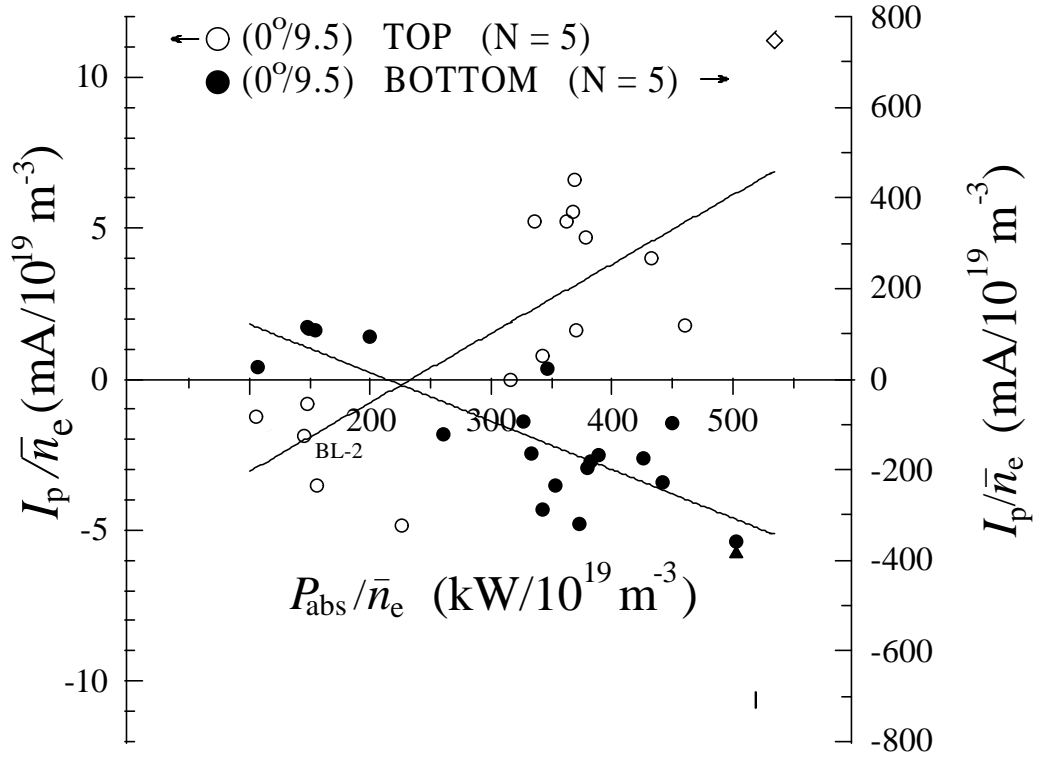


Fig. 8

(a)



(b)

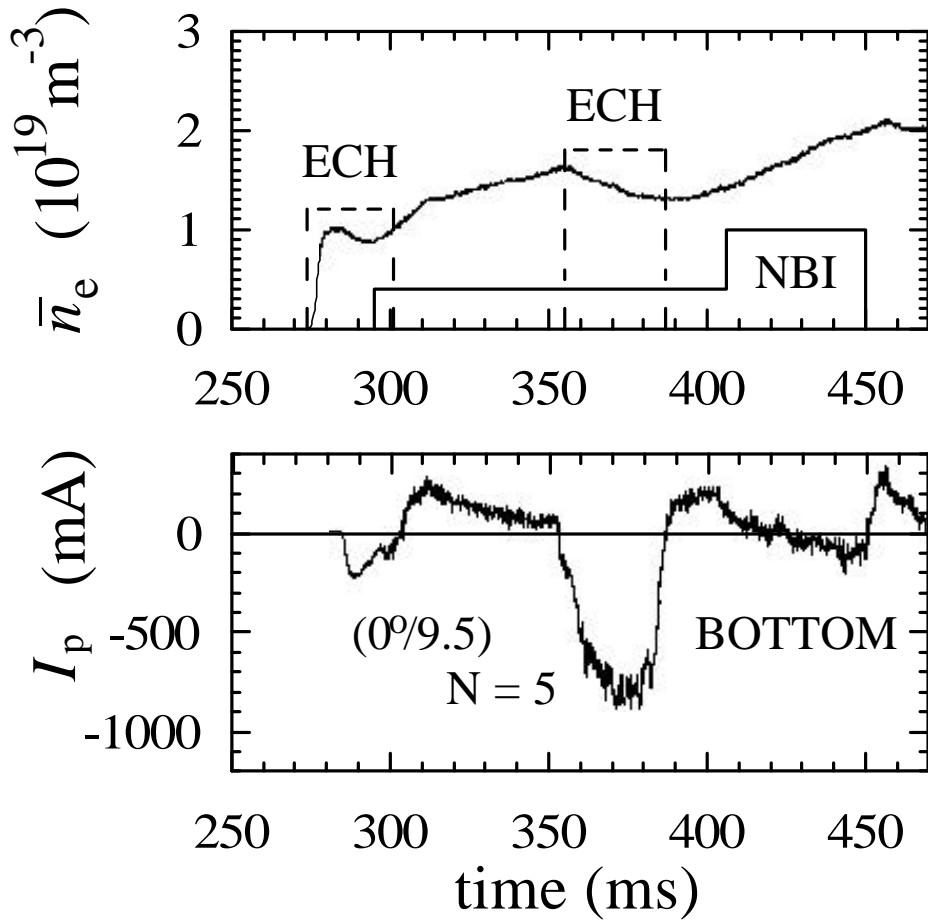


Fig. 9

(90°/9.5) OUTBOARD

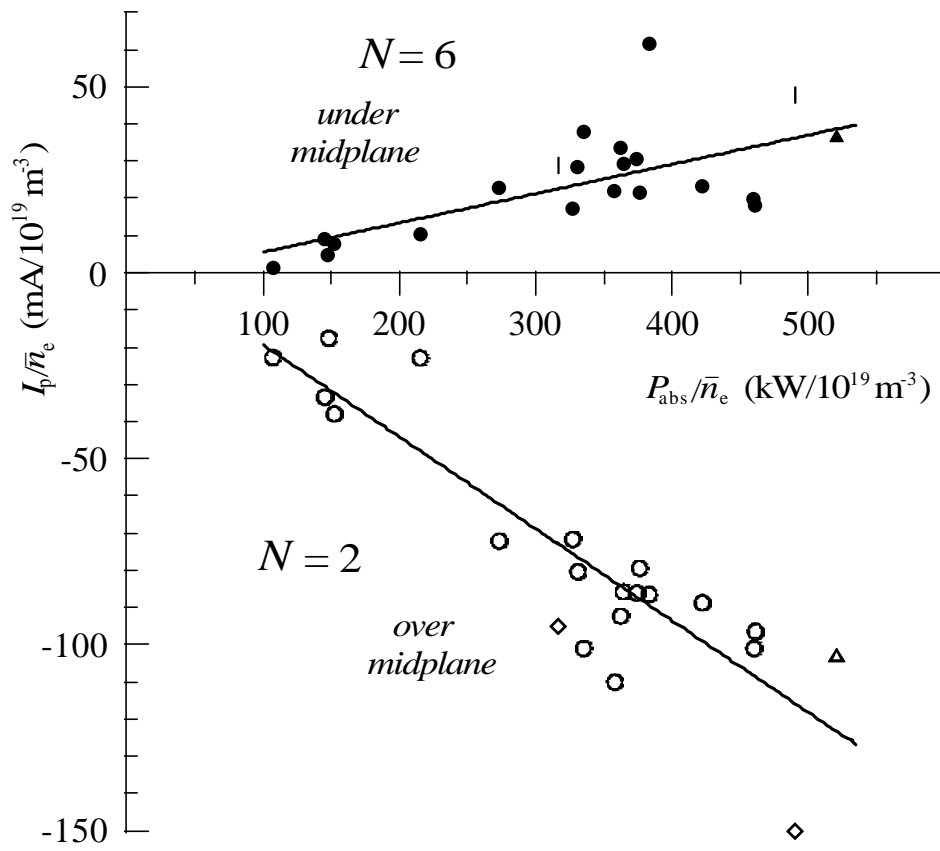


Fig. 10

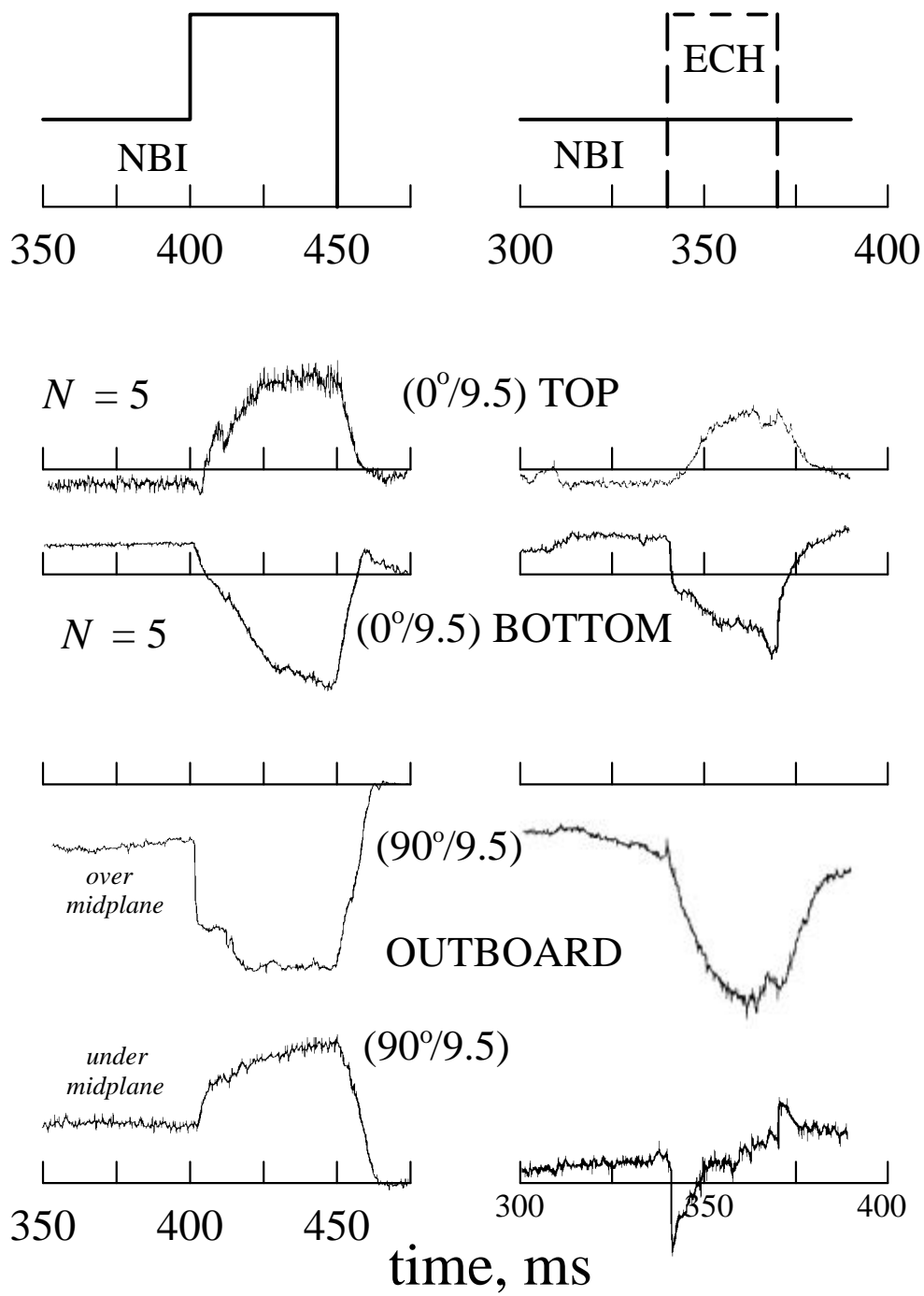
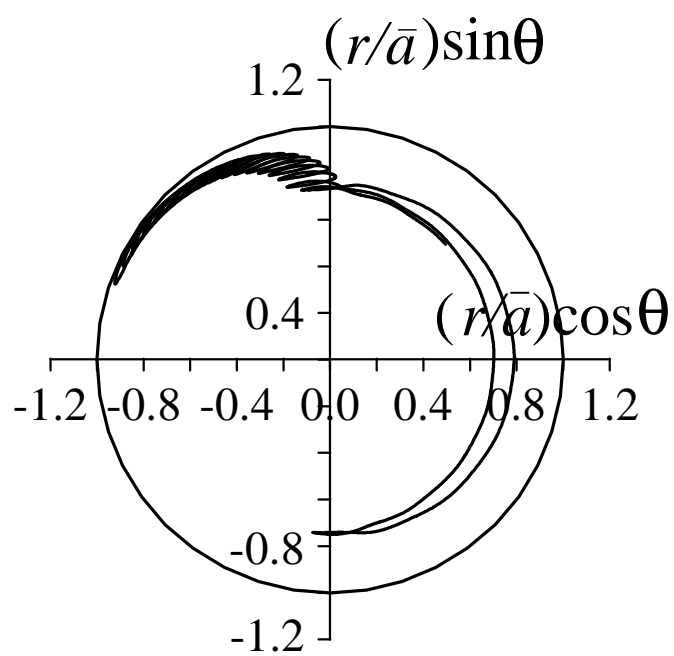


Fig. 11

(a)



(b)

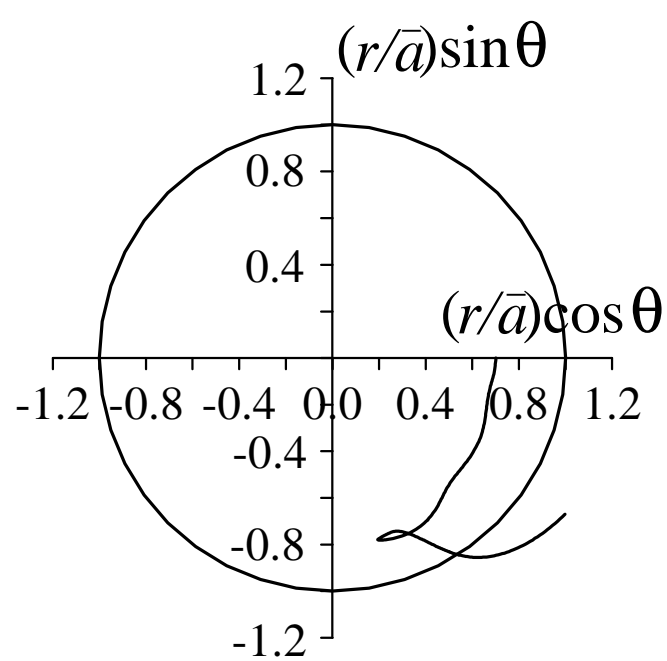


Fig. 12

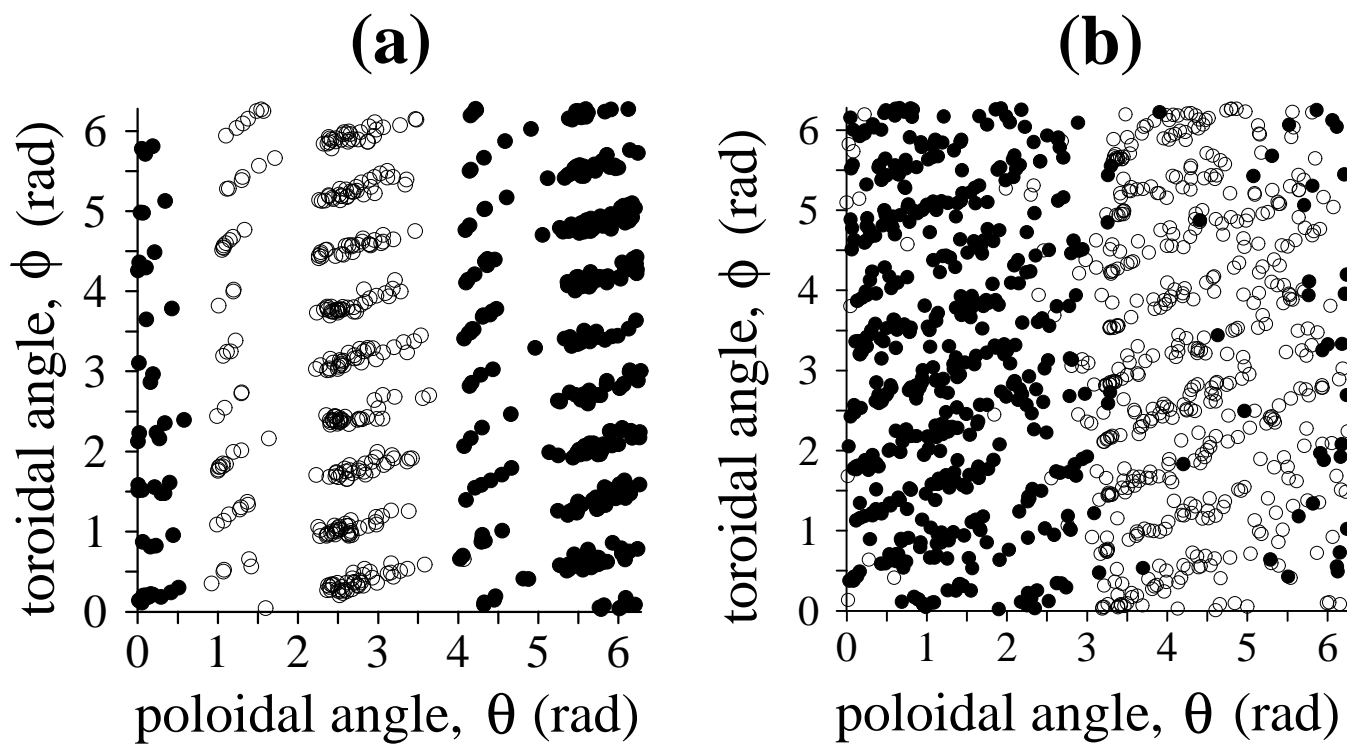


Fig. 13

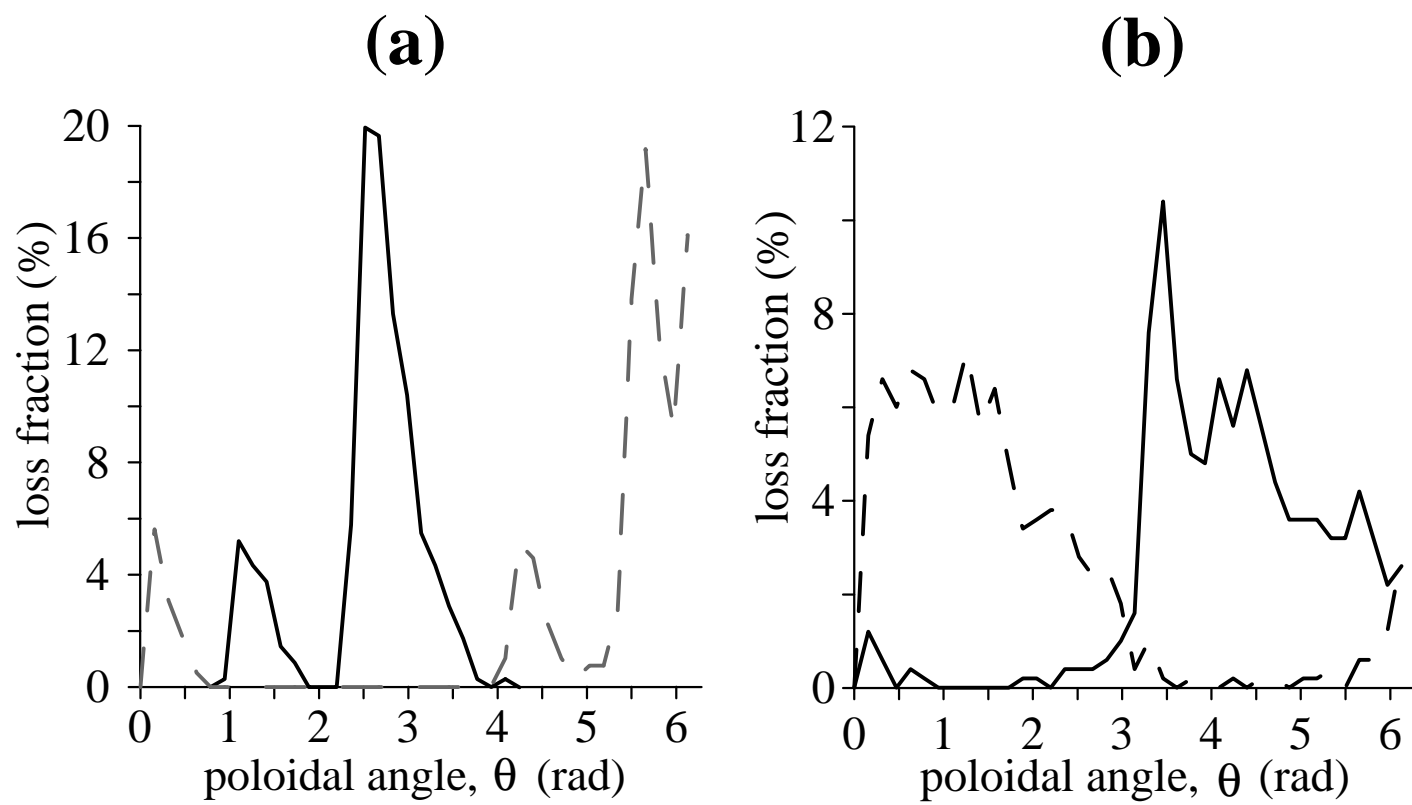


Fig. 14

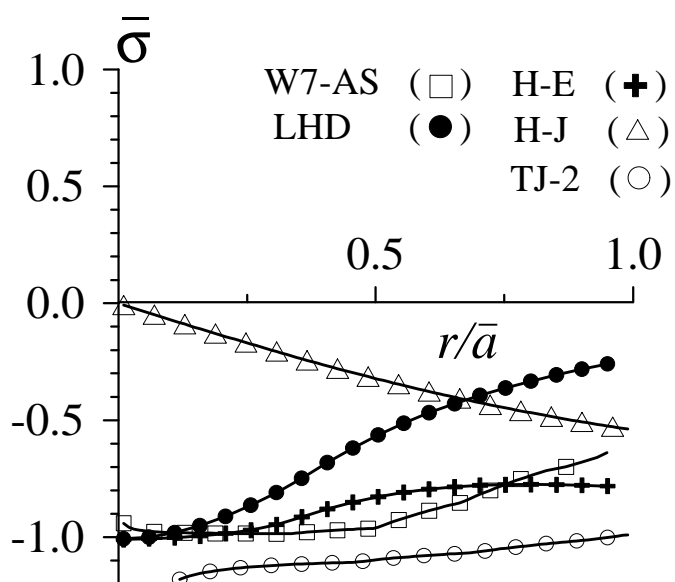
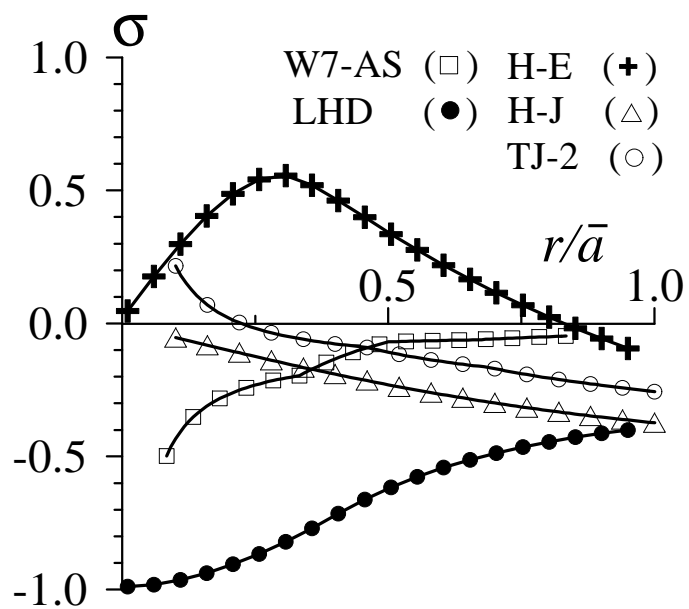


Fig.15

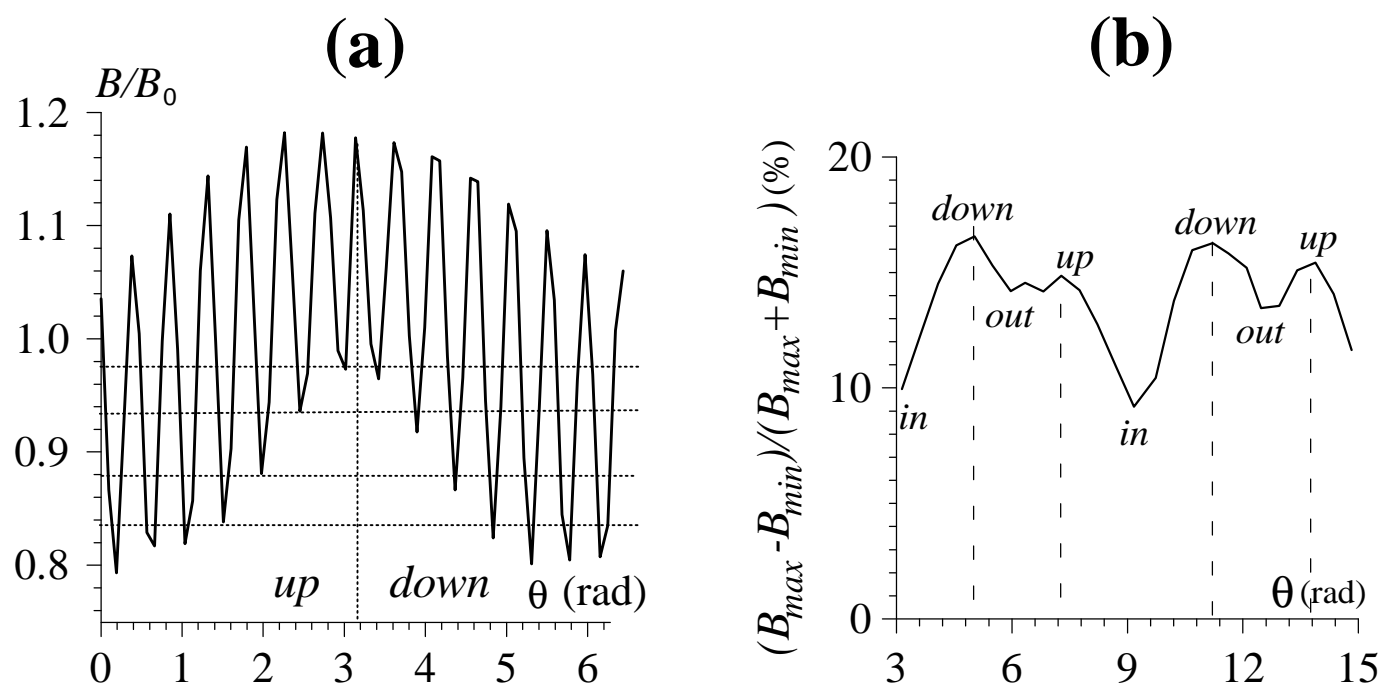


Fig. 16

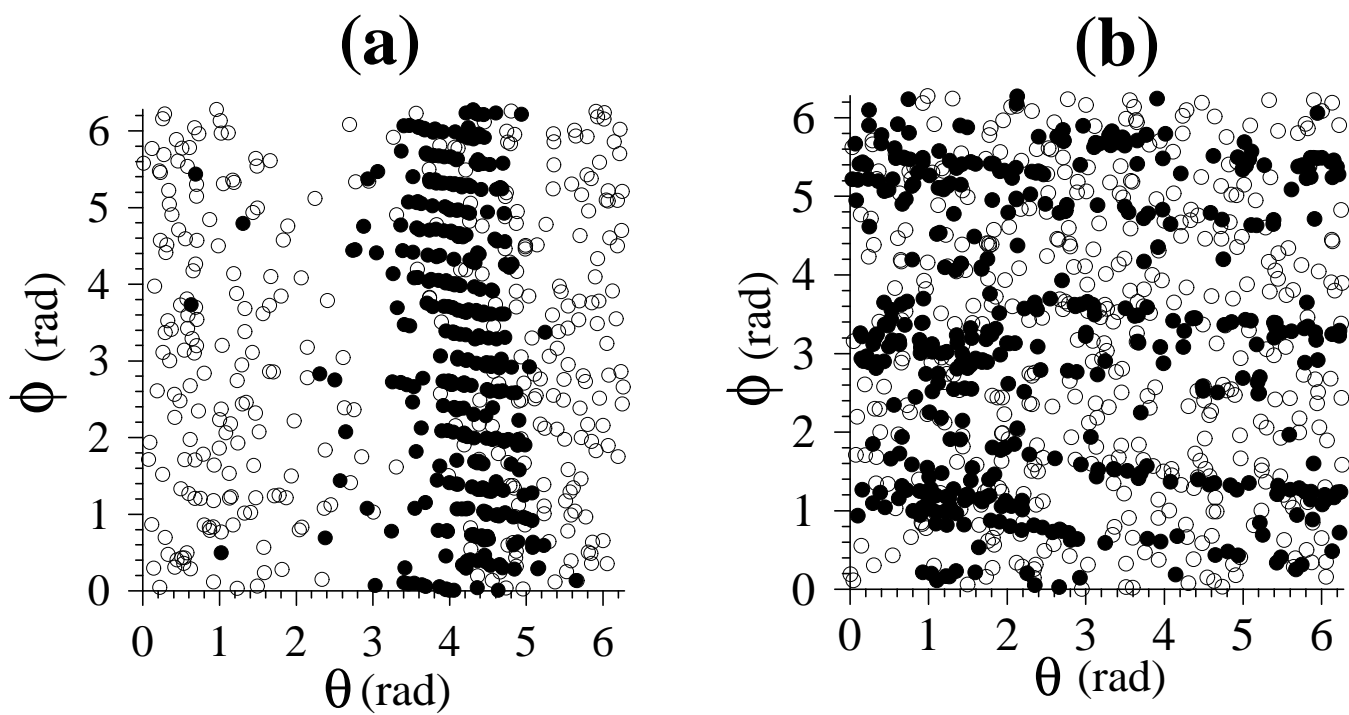


Fig. 17

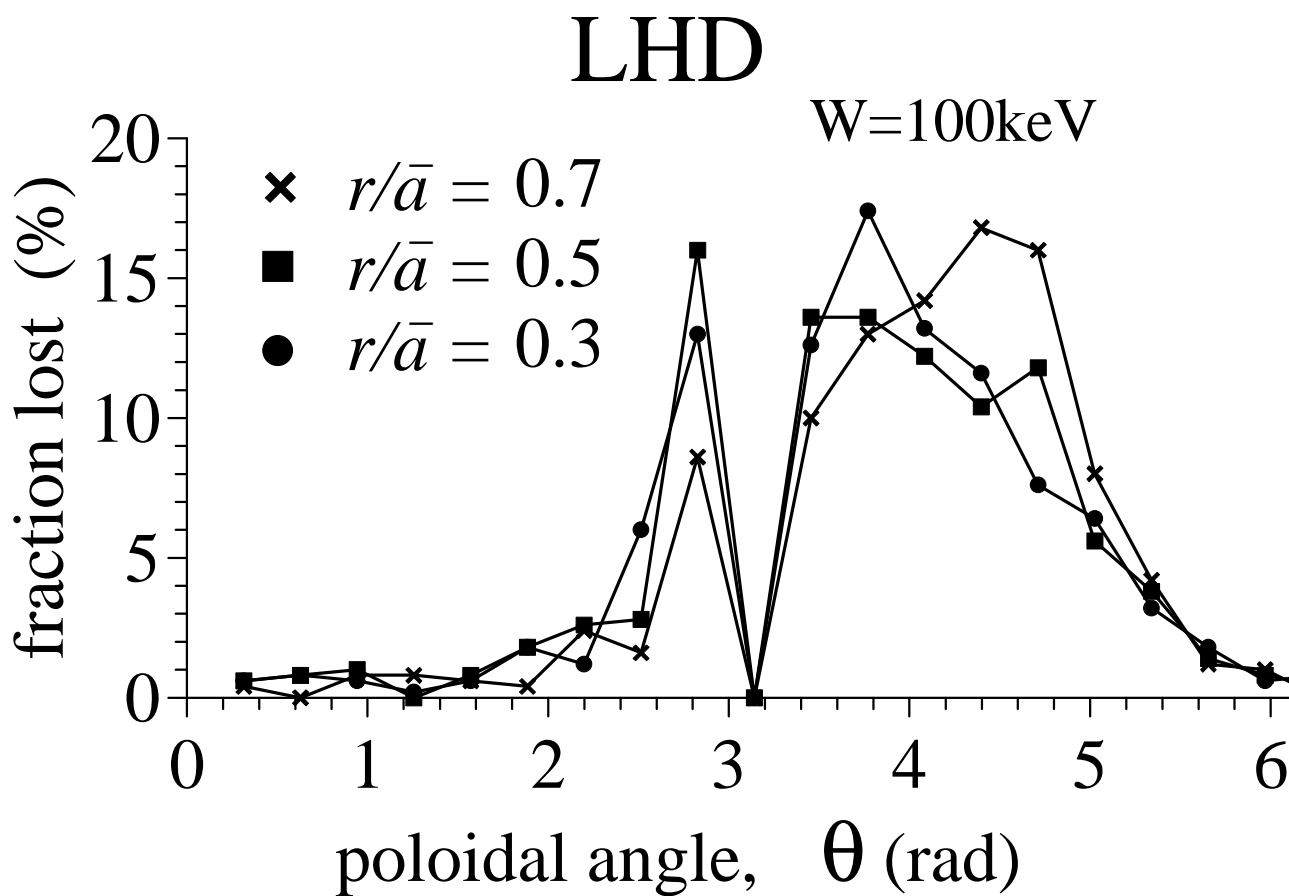
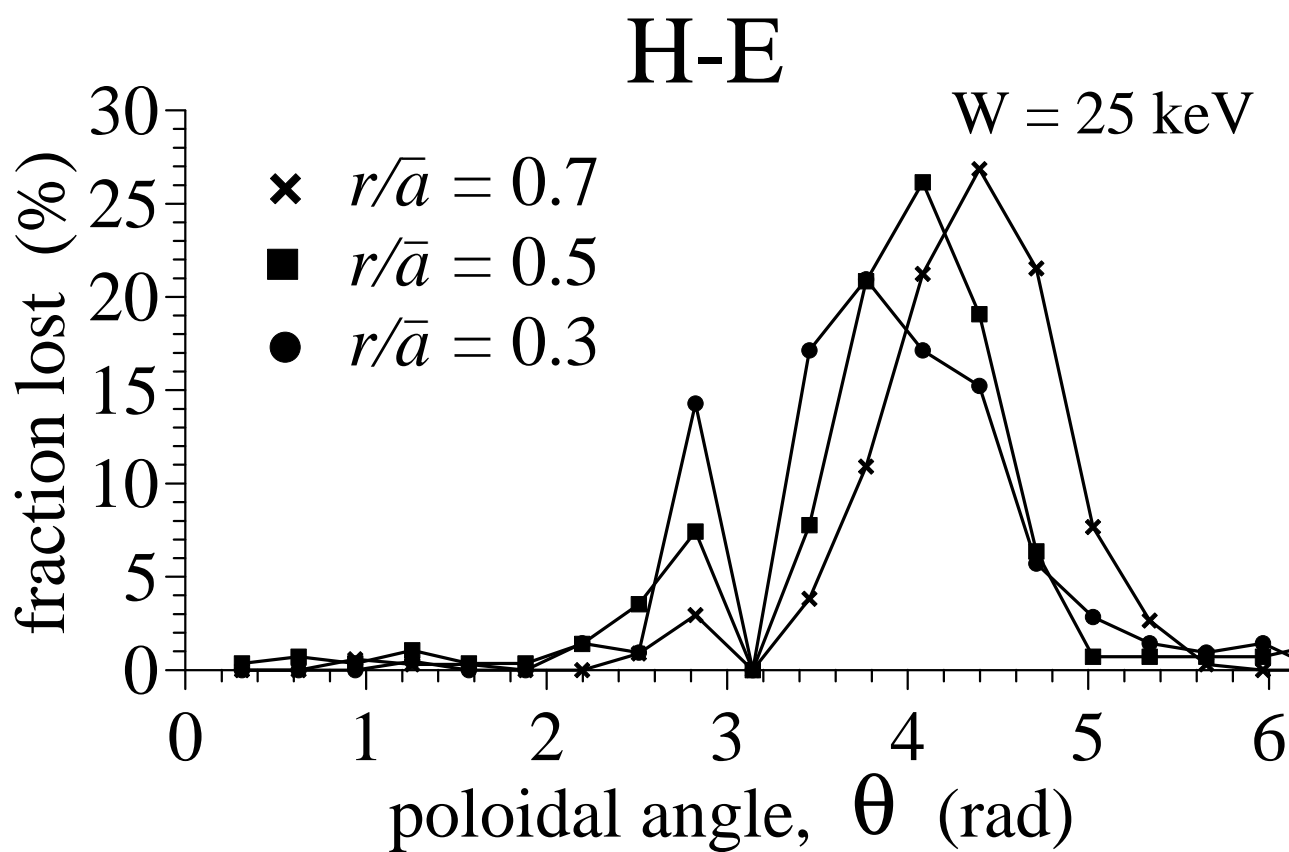


Fig. 18

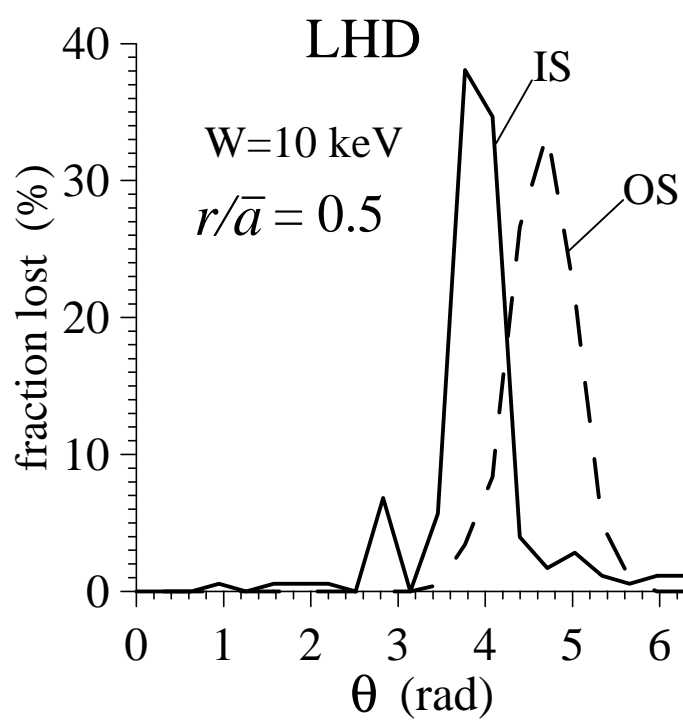


Fig. 19

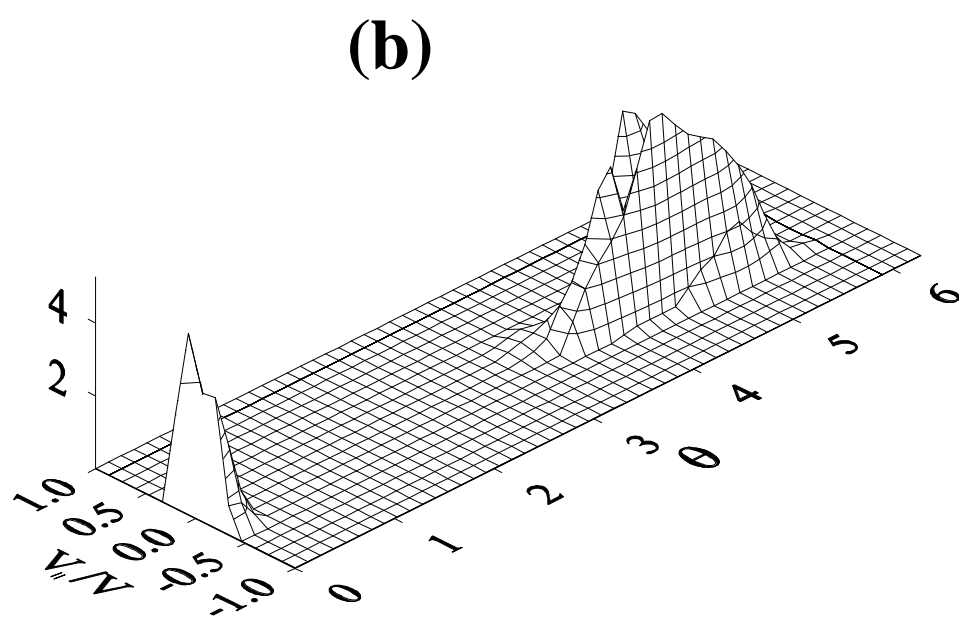
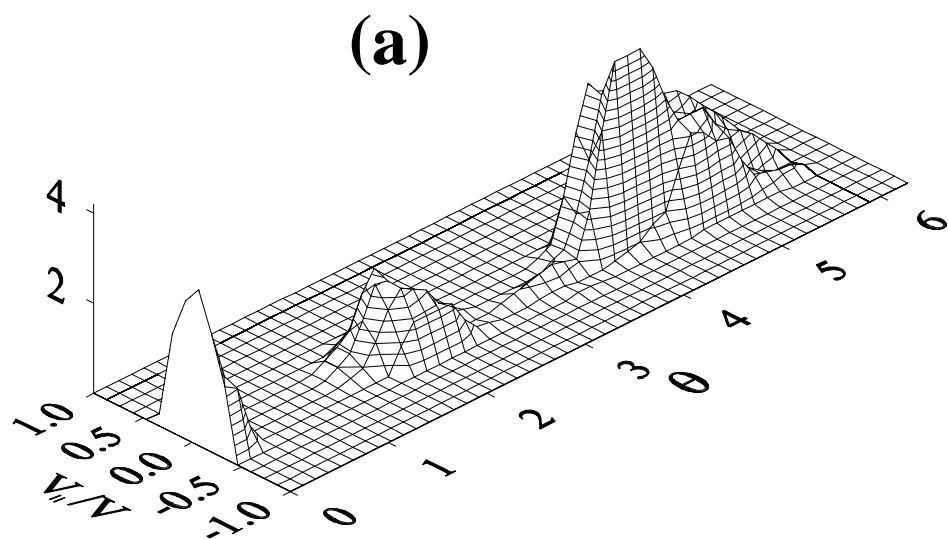


Fig. 20